Environmental controls on the brGDGT and brGMGT distributions across the Seine River basin (NW France): Implications for bacterial tetraethers as a proxy for riverine runoff

Zhe-Xuan Zhang[1,2], Edith Parlanti[2], Christelle Anquetil[1], Jérôme Morelle[3], Anniet M. Laverman[4], Alexandre Thibault[5], Elisa Bou[6], Arnaud Huguet[1*]

1. Sorbonne Université, CNRS, EPHE, PSL, UMR METIS, Paris, 75005, France
2. Univ. Bordeaux, CNRS, Bordeaux INP, EPOC, UMR 5805, F-33600 Pessac, France
3. Department of Biology and CESAM – Centre for Environmental and Marine Studies, University of Aveiro, Campus de Santiago, Aveiro, 3810-193, Portugal
4. Univ. Rennes 1, CNRS, ECOBIO-UMR 6553, Rennes, 35000, France
5. Antea Group, Innovation Hub, 803 boulevard Duhamel du Monceau, Olivet, 45160, France
6. Université de Toulouse, CNRS, Toulouse INP, Université Toulouse 3 - Paul Sabatier (UPS), Laboratoire Ecologie Fonctionnelle et Environnement, Route de Narbonne 118, Toulouse, 31062, France

Abstract

Branched glycerol dialkyl glycerol tetraethers (brGDGTs) are bacterial lipids that have been largely used as environmental proxies in continental paleorecords. Another group of related lipids, branched glycerol monoalkyl glycerol tetraethers (brGMGTs), has recently been proposed as a potential paleotemperature proxy. Nevertheless, the sources and environmental dependencies of both brGDGTs and brGMGTs along the river-sea continuum are still poorly understood, complicating their application as paleoenvironmental proxies in aquatic settings. In this study, the sources of brGDGTs and brGMGTs and the potential factors controlling their distributions are explored across the Seine River basin (NW France), which encompasses the freshwater to seawater

* Corresponding author. Tel: + 33-144-275-172; fax: +33-144-275-150.
E-mail address: arnaud.huguet@sorbonne-universite.fr (A. Huguet).

continuum. To this aim, brGDGTs and brGMGTs were analyzed in soils, Suspended Particulate Matter (SPM) and sediments (*n*=237) collected all along this basin, from land to sea. Both types of compounds are shown to be produced *in situ*, in freshwater as well as saltwater. Redundancy analysis further shows that both salinity and nitrogen loadings dominantly control the brGDGT distributions. Furthermore, the relative abundance of 6-methyl *vs*. 5-methyl brGDGTs (IR_{6Me} ratio), Total Nitrogen (TN), $\delta^{15}N$ and chlorophyll *a* concentration co-vary in the upstream area, suggesting that 6-methyl brGDGTs are preferentially produced under low-salinity and high-productivity conditions. In contrast with brGDGTs, brGMGT distribution appear to be primarily regulated by salinity, with a distinct influence on the individual homologues. Salinity is positively correlated with homologues H1020a and H1020b, and negatively correlated with compounds H1020c, H1034b, and H1034c. This suggests that bacteria thriving in freshwater preferentially produce compounds H1020c, H1034b, and H1034c, whereas bacteria primarily growing in saltwater appear to be predominantly responsible for the production of homologues H1020a and H1020b. Based on the abundance ratio of the freshwater-derived compounds (H1020c, H1034b, and H1034c) *vs.* saltwater-derived homologues (H1020a and H1020b), a novel proxy, Riverine Index (RIX) is proposed to trace riverine organic matter inputs, with high values (>0.5) indicating higher riverine contribution. As RIX relies on compounds that are specifically produced in certain settings (freshwater or saltwater), this index has potential to serve as a powerful proxy for riverine runoff in modern samples as well as in paleorecords.

Keywords: branched GDGTs; branched GMGTs; environmental proxies; land-ocean continuum; riverine runoff

1. Introduction

Branched glycerol dialkyl glycerol tetraethers (brGDGTs) are membrane lipids produced by unknown bacteria, although some of them were attributed to the phylum *Acidobacteria* (Sinninghe Damsté et al., 2011; Chen et al., 2022; Halamka et al., 2022). These compounds were observed to occur ubiquitously in a wide range of terrestrial and aquatic environments (Schouten et al., 2013; Raberg et al., 2022). The distribution of brGDGTs (number of cyclopentane moieties and methyl groups; cf. structures in Fig. S1) was empirically linked with pH and Mean Annual Air Temperature (MAAT) in soils (Weijers et al., 2007; De Jonge et al., 2014; Véquaud et al., 2022), peats (Naafs et al., 2017; Véquaud et al., 2022) and lake sediments (Martínez-Sosa et al., 2021). The brGDGT-based proxies (i.e. MBT'$_{5ME}$ and CBT') have been largely applied to reconstruct MAAT and pH from sedimentary archives (Coffinet et al., 2018; Harning et al., 2020; Wang et al., 2020).

In aquatic settings, brGDGTs were initially suggested to be predominantly derived from watershed soils and transported by erosion in the sediments (Hopmans et al., 2004). Based on this assumption, the Branched and Isoprenoid Tetraethers (BIT) index was defined as the abundance ratio of the major brGDGTs to crenarchaeol (isoprenoid GDGT mainly produced by marine *Thaumarchaeota*). It is comprised between 0 and 1, with high BIT values (around 1) reflecting higher contribution of terrestrial organic matter compared to marine organic matter (Hopmans et al., 2004). Over the last years, the BIT index has been broadly used for quantifying the relative contribution of terrestrial organic matter in aquatic systems (Xu et al., 2020; Yedema et al., 2023) and evaluating the reliability of TEX_{86} palaeothermometer (Cramwinckel et al., 2018). However, several studies have shown that brGDGTs can also be produced *in situ* in aquatic settings (Peterse et al., 2009; Tierney and Russell, 2009; Zell et al., 2014; De Jonge et al., 2015; Zhang et al., 2020),

adding complication for the identification of brGDGT sources in these ecosystems and for the application of the brGDGTs as (paleo)environmental proxies, including the BIT index. The BIT values have all the more to be carefully interpreted as they could also be influenced by the selective degradation of branched *vs*. isoprenoid GDGTs (Smith et al., 2012). Thus, complementary molecular proxies for quantifying the input of terrestrial organic matter to aquatic settings is still needed.

The improvement of analytical methods allowed the separation and quantification of 5-, 6- and 7-methyl brGDGTs (methyl groups at the fifth, sixth, and seventh positions; Fig. S1), that in previous chromatographic protocols co-eluted (De Jonge et al., 2014, 2013; Ding et al., 2016). Compounds eluting later than 7-methyl brGDGTs are tentatively designated 1050d and 1036d, as their exact chemical structures are currently unknown (Wang et al., 2021). The fractional abundance of the individual brGDGT isomers was shown to be influenced by distinct environmental factors. For example, the relative abundance of 5-methyl brGDGTs was correlated with temperature, whereas one of 6-methyl brGDGTs was correlated with pH (De Jonge et al., 2014). In addition to temperature and pH, other environmental factors may influence brGDGT distributions in terrestrial and aquatic settings and hence the application and interpretation of brGDGT-derived proxies. For example, recent studies in lakes observed an influence of salinity on the relative abundance of 6-methyl, 7-methyl brGDGTs and their late-eluting compounds (Wang et al., 2021; Kou et al., 2022). This suggests that salinity could also control the distribution of these compounds in other systems like river-sea continuums but this assumption has not yet been studied.

Compared with brGDGTs, the branched glycerol monoalkyl glycerol tetraethers (brGMGTs) are a much less studied group of lipids. Recent studies have revealed their presence in diverse environments, including peatlands (Naafs et al., 2018), marine settings (Liu et al., 2012),

rivers (Kirkels et al., 2022a) and lakes (Baxter et al., 2021, 2019). BrGMGTs are labelled as H1020, H1034, and H1048 respectively (cf. Fig. S1), with isomers suggested by a suffix letter (a-c) following the order in which they elute according to Baxter et al. (2019). These compounds are structurally similar to brGDGTs, but possess an additional covalent carbon–carbon bond between the alkyl chains, leading to "H-shaped" structure. The bridge of brGMGTs was considered to be a primary adaptation to heat stress (Naafs et al., 2018; Baxter et al., 2019). Although a rigorous chemical characterization of brGMGTs is lacking and the source organisms of brGMGTs are unknown, correlations between the relative abundances of brGMGTs and MAAT were observed in peat soils (Naafs et al., 2018) and lakes (Baxter et al., 2019), showing their potential as temperature proxies. In addition to temperature, shifts in microbial community composition in response to other unknown environmental factors seem to control the relative abundances of brGMGTs in peats and lignites (Elling et al., 2023). Henceforth, in order to use the brGMGT as environmental proxies in sedimentary records, it is still necessary to understand which factors control their distributions in riverine and marine water columns and sediments, which remain to date unclear (Bijl et al., 2021; Sluijs et al., 2020).

Based on previous studies of brGDGTs and brGMGTs in terrestrial and marine settings (Dearing Crampton-Flood et al., 2019; Wang et al., 2021; Kirkels et al., 2022a, 2022b; Kou et al., 2022), we hypothesize (1) that both brGDGTs and brGMGTs can be produced *in situ* in aquatic systems and (2) that brGDGT and brGMGT distribution are influenced by surrounding environmental factors and vary spatially along the land-sea continuum. These compounds have a potential to be used as proxies of riverine organic matter inputs along estuaries. These hypotheses were tested by examining and comparing the distribution of brGDGTs and brGMGTs in soils, suspended particulate matter (SPM) and sediments (n = 237) collected all along the Seine River

basin (NW France), covering its riverine and estuarine parts. The aim of the present study was (1) to investigate the sources of brGDGTs and brGMGTs along the Seine land-sea continuum, (2) to determine the predominant environmental controls affecting the distribution of these molecules and (3) to assess the potential of brGMGTs as a riverine runoff proxy.

2. Material and methods

2.1. Study area

The Seine River basin (Seine River and its estuary; Fig. 1a) is more than 760km long and is characterized by high population density, draining through the greater Paris region (over 12 million inhabitants) to the English Channel (Flipo et al., 2021). The Seine Estuary is a macrotidal estuary according to its high tidal range, small depth and morphology. The maximum flows are generally observed in winter (over 700 m^3/s; Fig. 1b), whereas the minimum flows are observed in summer (below 250 m^3/s; Fig. 1b). The tide influences the estuary up to the city of Poses (site 5, KP 202 in Fig. 1a; KP represents kilometric point and is defined as the distance in kilometers from the city of Paris), where a dam constitutes the boundary between the river and the estuary. The estuary can be divided into two major parts: the upstream section mainly influenced by freshwater (KP 202 to KP 298, from site 5 to site 12; Fig. 1a and Table 1) and the downstream section predominantly influenced by saltwater intrusion (starting at KP 298, from site 12 to the coastal area; Fig. 1a and Table 1).

2.2. Sampling

From June 2019 to March 2021, water samples (n=102) were collected across the Seine River (Fig. 1a). Sub-surface water (ca. 1m depth) samples were collected in high-flow (over

250 m^3/s) and low-flow (below 250 m^3/s) seasons from the three zones (river, upstream estuary and downstream estuary) of the Seine River basin (Table 1). At 5 sites (sites 4, 6, 10, 13, and 15, Fig. 1a and Table 1), both sub-surface and bottom water (2.2-16m depth) samples were retrieved using a pump into precleaned 20L FLPE Nalgene carboys. Estuarine water samples (sites 6, 10, 13, and 15; Fig. 1a and Table 1) were collected at three tide periods (high tide, low tide and mid tide). For these sites, 0.25-43L of water were immediately filtered using pre-combusted Whatman GF/F 0.7 µm glass fiber filters. After filtration, filters were freeze-dried, scratched and stored frozen at -20°C prior to analysis.

Additional SPM samples (*n*=16; Table 1) used in this study for brGDGT and brGMGT analysis were collected from the upstream and downstream estuary (site 5, 7, 13, 15, 17, 18, and 19; Fig. 1a and Table 1) in 2015 and 2016, as detailed by Thibault et al. (2019). Sediments (*n*=68) from 8 cores (10cm depth) were collected at the same sites as these SPM samples in 2015 and 2016 using a UWITEC corer as described by Thibault et al. (2019) (Table 1). These sediments were further sliced (1-cm thickness) and freeze-dried. Surficial soils (*n*=9) were collected in the lateral area of the upstream section of the Seine river in 2021 (site A, B, and C, Fig. 1a and Table S1) and freeze-dried. Additional wetland soils and mudflat sediments (*n*=42) were collected in the downstream estuary in 2018, 2020, and 2021 (site D and E, Fig. 1a and Table S1), representing allochtonous material transported into the estuary by tidal effect. These samples were collected at low tide using a plexiglass® core (4.5 cm depth), and back to the laboratory, homogenized, freeze-dried, and ground using a ball mill (model MM400, Retsch®)

2.3. Elemental and isotopic analyses

Elemental and isotopic analyses of the soils (surficial soils and mudflat sediments, *n*=51) and SPM (*n*=102) collected from 2018 to 2021 were performed following the method described in

Thibault et al. (2019). Briefly, 40 mg of SPM and 1 g of soils/sediments samples were firstly decarbonated by adding 10 mL of 3 M HCl for 2 h with magnetic stirring at room temperature. Subsequently, these samples were rinsed using ultrapure water and centrifuged until reaching neutral pH. The obtained decarbonated samples were stored at −20 °C and freeze dried. Both decarbonated and non-decarbonated samples (~6 mg for SPM and ~20 mg for soils) were enclosed in a tin capsule. Total Organic Carbon content (TOC) and stable carbon isotopic composition ($\delta^{13}C$) were measured in decarbonated samples using an elemental analyzer coupled with an isotope ratio mass spectrometer (Thermo Fisher Scientific Delta V Advantage) at the ALYSES platform (Sorbonne University / IRD, Bondy, France). Total Nitrogen (TN) and nitrogen isotope ($\delta^{15}N$) were measured in non-decarbonated samples as acidification could impact the N contents (Ryba and Burgess, 2002). The isotopic composition ($\delta^{13}C$ or $\delta^{15}N$) was expressed as relative difference between isotopic ratios in samples and in standards (Vienna Pee Dee Belemnite for carbon or atmospheric N_2 for nitrogen). Additional elemental and isotopic analyses of SPM and sediments collected in 2015 and 2016 (*n*=84) were carried out as described in Thibault et al. (2019).

2.4. Lipid extraction and analyses

The lipids from surficial soils and mudflat sediments (4-20g, *n*=51), and from SPM samples (~150mg, *n*=102) were extracted ultrasonically (3×) with 20 to 40 mL of dichloromethane (DCM): methanol (MeOH) (5/1, v/v) per extraction. Lipids from the SPM and sediments samples (*n*=84) collected in 2015 and 2016 were previously extracted by Thibault (2018) following the same method. The total lipid extracts were then separated into fractions of increasing polarity on an activated silica gel column, using (i) 30 mL of heptane, (ii) 30 mL of heptane:DCM (1/4, v/v), and (iii) 30 mL of DCM/MeOH (1/1, v/v) as eluents. An aliquot (30%) of the third (polar) fraction containing GDGTs and GMGTs was dried, re-dissolved in heptane, and passed through a 0.2μm

polytetrafluoroethylene (PTFE) filter (Ultrafree-MC; Merck). C_{46} Glycerol Trialkyl Glycerol Tetraether (GTGT) was used as an internal standard (Huguet et al., 2006). 5 µl of this standard (0.01025 mg/mL) was typically added to 45 µl of sample.

GDGTs and GMGTs were analyzed using a Shimadzu LCMS 2020 high pressure liquid chromatography coupled with mass spectrometry with an atmospheric pressure chemical ionization source (HPLC-APCI-MS) in selected ion monitoring mode, modified from Hopmans et al. (2016) and Huguet et al. (2019). Tetraether lipids were separated with two silica columns in tandem (BEH HILIC columns, 2.1 × 150 mm, 1.7 µm; Waters) thermostated at 30°C. Injection volume was 30 µL. The flow rate was set at 0.2 mL/min. GDGTs and GMGTs were eluted isocratically for 25 min with 82% A/18% B (A= hexane, B=hexane/isopropanol 9/1, v/v), followed by a linear gradient to 65% A/35% B in 25 min, then a linear gradient to 100% B in 30 min, and back to 82% A/18% B in 4 min, maintained for 50 min. Semi-quantification of brGDGTs and brGMGTs was performed by comparing the integrated signal of the respective compound with the signal of a C_{46} synthesized internal standard (Huguet et al., 2006) assuming their response factors to be identical.

2.5. Calculation of GDGT proxies

The IR_{6Me} index represents the proportion of 6-methyl brGDGTs *vs*. 5-methyl brGDGTs and was calculated according to De Jonge et al. (2015; Eq. 1) with Roman numbers referring to the structures in annex (Fig. S1):

$$IR_{6Me} = \frac{II_{a_6}+II_{b_6}+II_{c_6}+III_{a_6}+III_{b_6}+III_{c_6}}{II_{a_5}+II_{b_5}+II_{c_5}+II_{a_6}+II_{b_6}+II_{c_6}+III_{a_5}+III_{b_5}+III_{c_5}+III_{a_6}+III_{b_6}+III_{c_6}} \quad (1)$$

The BIT index including the 6-methyl brGDGTs was calculated following De Jonge et al. (2015; Eq. 2):

$$\mathrm{BIT} = \frac{\mathrm{I_a}+\mathrm{II_{a_5}}+\mathrm{II_{a_6}}+\mathrm{III_{a_5}}+\mathrm{III_{a_6}}}{\mathrm{I_a}+\mathrm{II_{a_5}}+\mathrm{II_{a_6}}+\mathrm{III_{a_5}}+\mathrm{III_{a_5}}+\mathrm{crenarchaeol}} \quad (2)$$

Based on duplicate injections, the average analytical error was 0.005 for IR_{6Me} and 0.06 for BIT.

2.7. Water quality measurements

Water turbidity was measured by a CTD Probe Sea-bird®. Water temperature, dissolved oxygen, salinity, and pH were measured using an automated YSI 6000 multi-parameter probe (YSI inc., Yellow springs, OH, USA). Chlorophyll *a* (Chl *a*) concentrations were measured on water samples after filtration on Whatman GF/F 0.7 µm glass fiber filters, which were stored frozen (-20° C) before analysis. Chl *a* was extracted from filters with incubation in 10 ml of 90% acetone for 12 hours in the dark at 4°C. After two centrifugations (1700 g, 5 min), Chl *a* concentrations were measured using a Turner Designs Fluorometer according to the method of Strickland and Parsons (1972) as described in the reference protocol of SNO SOMLIT (Service d'observation du Milieu Littoral).

2.8. Statistical analyses

All statistical analyses were performed using the R software (version 4.2.1). The non-parametric statistical tests were used due to the non-normal distribution of the dataset (tested by Shapiro–Wilk normality test; p-values < 0.05). Specifically, the Spearman's correlation was used to investigate potential correlations among different features (environmental parameters, fractional abundances of brGDGTs and brGMGTs, and proxies derived from these compounds), and the unpaired two-samples Wilcoxon test (also known as Mann-Whitney test or Wilcoxon rank sum test) was used for two independent group comparisons. Significance level is indicated by asterisks: *p-value < 0.05; **p-value < 0.01; ***p-value < 0.001; ****p-value < 0.0001; NS (not significant), p-value > 0.05.

A Principal Component Analysis (PCA) was performed on the fractional abundances of brGDGTs and brGMGTs, using the R packages factoextra and FactoMineR. The different groups of samples were highlighted by adding 95% concentration ellipses. The proportion of variance in brGDGT and brGMGT compositions that can be explained by different groups was evaluated by permutational multivariate analysis of variance using distance matrices (adonis) in the adonis2 function of the R package Vegan, using the Bray-Curtis distances and 999 permutations.

A Redundancy analysis (RDA) was performed using the R package vegan to investigate the relationship between environmental parameters and brGDGT or brGMGT distributions in SPM. Angles between brGDGTs or brGMGTs and environmental factors were used to identify the potential correlations. Right angles (90°) reflect a lack of linear correlations, whereas small or straight angles (close to 0° or 180°, respectively) imply positive or negative linear correlations. The compounds that are close to each other were assumed to be strongly linked, representing similar distribution patterns and comparable responses to the environmental conditions. To evaluate the relative importance of each explanatory variable (environmental parameters) on brGDGT or brGMGT distributions, a hierarchical partitioning method implemented in the R package rdacca.hp was used. This method calculated the individual importance (sum of the unique and total average shared effects) from all subset models, generating an unordered assessment of variable importance (Lai et al., 2022).

Spatial-temporal variations of environmental factors and proxies derived from brGDGTs and brGMGTs were assessed after applying a locally estimated scatterplot smoothing (LOESS) method. This method allows the identification of nonlinear data patterns and buffers the effect of aberrant data and outliers. LOESS was implemented by the geom_smooth function of the R package ggplot2.

3. Results

3.1. Distribution of brGDGTs from land to sea

The different brGDGTs were detected in all studied samples (Table S1). The brGDGT chromatograms for downstream estuarine samples differed markedly from upstream samples (SPM and sediments).

The brGDGT chromatograms from upstream samples (SPM and sediments) differed markedly from downstream estuarine samples (SPM and sediments). For example, 6-methyl brGDGTs were much more abundant than 5-methyl brGDGTs in the river (SPM) and upstream estuary (SPM), whereas the strong predominance of 6-methyl *vs.* 5-methyl brGDGTs decreased in the downstream samples (Fig. 2). Furthermore, the peaks of the recently described 7-methyl brGDGTs and their late-eluting isomers (i.e. 1050d) were more pronounced in the downstream estuary than in the rest of the Seine basin (Fig. 2).

The relative abundances of the brGDGTs were determined all along the Seine River basin (Fig. 3 and Fig. S3). The 6-methyl brGDGTs ($IIIa_6$ and IIa_6) were significantly higher in river (SPM) and upstream estuary (SPM and sediments) than in soils (surficial soils and mudflat sediments) and downstream estuary (SPM and sediments). In addition, the relative abundances of 7-methyl brGDGTs ($IIIa_7$ and IIa_7) and their late-eluting compounds (1050d and 1036d) in downstream estuary (SPM and sediments) were significantly higher than those in the upstream estuary (SPM and sediments).

The concentration of total brGDGTs also showed differences along the land to sea continuum (Fig. S2 and Table S1). The total brGDGTs concentration decreased from river (10.51

± 5.91 μg/g organic carbon (C_{org}), based on SPM samples) to upstream estuary (7.52 ± 5.09 μg/g C_{org}, based on SPM and sediments) and downstream estuary (4.95 ± 4.09 μg/g C_{org}, based SPM and sediments). In soils (surficial soils and mudflat sediments) from all the Seine basin, the concentration in total brGDGTs was significantly lower than that in SPM and sediments (Fig. S2 and Table S1).

A Principal Component Analysis (PCA) was performed to statistically compare the fractional abundances of brGDGTs from different location (river, upstream and downstream estuary, based on SPM and sediments), which explained 40.9% of the variance in two dimensions, with negative loadings for most of the 6-methyl brGDGTs and positive loadings for the remaining brGDGTs (Fig. 4a). Samples from the downstream estuary clustered well apart from those from the river and upstream parts. Specifically, the brGDGT distribution was dominated by 6-methyl brGDGTs ($IIIa_6$, $IIIb_6$, $IIIc_6$, IIa_6, and IIb_6) in river and upstream estuarine samples, whereas in downstream estuary, it was driven by 5-methyl brGDGTs (III_5, IIa_5, IIc_5, IIb_5, $IIIb_5$), tetramethylated brGDGTs (Ia, Ib, and Ic), 7-methyl brGDGTs ($IIIa_7$, IIa_7, and IIb_7), and their late-eluting compounds (1050d and 1036d).

A Redundancy analysis (RDA) was performed to investigate the influence of the environmental factors (TOC, TN, temperature, and salinity) on the brGDGT distributions in SPM samples (Fig. 5 and Table S2), which allowed to explain 38.9% of the variability through two dimensions. The RDA triplot (Fig. 5a) showed how these factors correlate to the distributions of individual brGDGTs. The first axis of the RDA explained 33.01% of the variability and was primarily correlated with salinity and TN, whereas the second axis explained 5.89% of the variability and was associated with temperature and TOC (Fig. 5a and Table S2). The first axis of the RDA explained 33.01% of the variability and was primarily correlated with salinity (15.2%)

306 and TN (13.8%), whereas the second axis explained 5.89% of the variability and was associated
307 with temperature and TOC (< 6% of the variance; Fig. 5 and Table S2).

308 *3.2 Distribution of brGMGTs from land to sea*

309 The seven brGMGTs identified in previous studies were all detected in the samples
310 collected across the Seine River basin (Fig. 2; Table S1). The chromatograms revealed distinct
311 distributions in brGMGTs in the different parts of the basin (SPM and sediments), with e.g. a higher
312 intensity for the homologue H1020c in the river samples (SPM) than in those from the upstream
313 (SPM) and downstream estuary (SPM) (Fig. 2). These spatial variations were apparent when
314 calculating the fractional abundances of the individual brGMGTs (Fig. 6). From upstream to
315 downstream, the relative abundances in H1020a and H1020b increased, whereas those in 1020c,
316 H1034b, and H1034c decreased (Fig. 6). In SPM and sediments, the total brGMGT concentration
317 was observed to be slightly higher in the riverine part (0.26 ± 0.17 μg/g C_{org}) than in downstream
318 (0.20 ± 0.14 μg/g C_{org}) and upstream estuary samples (0.18 ± 0.15 μg/g C_{org}; Fig. S2 and Table S1).
319 The total brGMGT concentrations were the lowest in soils all over the basin (0.07 ± 0.23 μg/g C_{org}).

320 The PCA analysis based on the brGMGT relative abundances (Fig. 4b) explained 70.2% of
321 the variance, which allows to observe that samples from the different parts of the basin clustered
322 well apart from each other. The first axis explained 55.1% of the variance, separating downstream
323 samples from riverine and upstream samples, with negative loadings for two brGMGTs (H1020a
324 and H1020b), and positive loadings for the remaining brGMGTs (H1020c, H1034a, H1034b,
325 H1034c, and H1048). The second axis explained 15.1% of the variance and mainly separated the
326 riverine and upstream samples (Fig. 4b), with higher relative abundances of compounds H1020c
327 and H1034b in riverine samples.

The RDA was performed to investigate the factors that could explain the variability of brGMGT distributions in SPM samples (Fig. 5 and Table S2), which allows to explain 25.39% of the variance. The RDA triplot showed that the first axis, accounting for 21.59% of the variability, was mainly associated with salinity and to a lesser extent TN, while the second axis (3.8%) was mainly driven by temperature and TOC (Fig. 5a and Table S2). Based on hierarchical partitioning, salinity had the highest variable importance and contributed to 13.22% of the brGMGT variations (Fig. 5d and Table S2). The brGMGTs were slightly influenced by TN and temperature, as these two factors contributed to 3.88% and 3.55% of brGMGT variations, respectively (Fig. 5d and Table S2).

4. Discussion

4.1. Sources of brGDGTs and environmental controls on their distribution

4.1.1 Sources of brGDGTs

In order to determine the predominant origin of brGDGTs in the Seine River basin, the overall brGDGT concentrations and distributions in SPM and sediments (n=186) were compared with those in soils (surficial soils and mudflat sediments, n=51). The brGDGT concentrations (normalized to C_{org}) and relative abundances of several brGDGTs (i.e. IIa_6 and $IIIa_6$) in the SPM and sediments are significantly higher than those in soils (p<0.05, Wilcoxon test; Fig. S2a and Fig. 3). Such differences in brGDGT concentrations and relative abundances between soils and aquatic settings (SPM and sediments) imply that at least part of the brGDGTs in the water column and sediments of the Seine River basin is produced *in situ*. This is in agreement with previous findings

which suggested an *in situ* aquatic contribution to the brGDGT pool (Crampton-Flood et al., 2021; De Jonge et al., 2015; Kirkels et al., 2022b; Peterse et al., 2009).

More specifically, the fractional abundances of the two major 6-methyl brGDGTs (IIa_6 and $IIIa_6$) are significantly higher in the Seine River and upstream estuary than in soils (Fig. 3). This confirms that these brGDGTs are mostly produced within the river, adding to the growing body of evidence supporting riverine 6-methyl brGDGT production (De Jonge et al., 2015; Bertassoli et al., 2022; Kirkels et al., 2022b). A subsequent shift in the brGDGT distributions in the downstream compared to the upstream areas is observed in the Seine River basin. The PCA analysis shows a separation of downstream estuarine samples (influenced by seawater intrusion) from riverine and upstream estuary ones (without significant seawater intrusion) (Fig. 4a). This difference is predominantly driven by the higher abundances of 6-methyl brGDGTs in riverine and upstream estuarine samples *vs.* higher abundances of 5- and 7-methyl brGDGTs as well as compounds Ib, Ic, and late eluting brGDGTs 1050d, 1036d in downstream estuarine samples (Figs. 3, 5a and A3). This difference suggests that riverine 6-methyl brGDGTs may be more easily degraded than other homologues and only partially transferred downstream. In addition to that, the riverine brGDGT signal may be diluted by brGDGTs from other sources during downstream transport. This is in agreement with a previous study, which showed a shift in brGDGT distribution from the Yenisei River to the Kara Sea (De Jonge et al., 2015). They interpreted this to be a preferential degradation of labile (riverine) 6-methyl brGDGTs and the enrichment in less labile (soil-derived) 5-methyl brGDGTs during transport (De Jonge et al., 2015). This suggests that only limited amounts of riverine 6-methyl brGDGTs are transferred to the ocean, as was also shown in other recent studies (Cao et al., 2022; Kirkels et al., 2022b). In addition, a shift in brGDGT distribution during downstream transport could be explained by mixing with autochthonous (i.e. estuarine-produced)

372 brGDGTs (Crampton-Flood et al., 2021). The relative abundance of several brGDGTs (i.e. Ib, Ic,
373 IIIa$_7$, IIa$_7$ and 1050d) in the downstream part of the Seine River basin is indeed significantly higher
374 than the one in the upstream part (p<0.05, Wilcoxon test; Fig. 3), suggesting *in situ* brGDGT
375 production in saltwater. Such a saltwater contribution can be visualized by the PCA based on
376 brGDGT distribution, showing the positive score of the aforementioned compounds with the first
377 axis (Fig. 4a). This axis is dominated by downstream samples influenced by seawater intrusion in
378 the Seine Estuary (Fig. 4a). However, it should be noted that the relative abundance of compounds
379 Ib, Ic, IIIa$_7$, IIa$_7$ and 1050d is roughly similar in soils and in downstream estuary samples (Fig. 3).
380 Hence, it cannot be excluded that these brGDGTs detected in downstream samples are at least
381 partly derived from soils of the watershed.

382 *4.1.2. Environmental controls on the brGDGT distribution*

383 As several individual brGDGTs are suggested to be preferentially produced either in the
384 riverine or estuarine parts of the Seine basin, their distribution might be related to ambient
385 environmental factors. The RDA (performed on SPM samples) highlights the relationships
386 between the available environmental variables (salinity, TN, TOC, and temperature) and the
387 relative abundances of brGDGTs. Hierarchical partitioning indicates that salinity is the most
388 important factor influencing the brGDGT distribution (15.2%) in the Seine River basin (Fig. 5b
389 and Table S2). Salinity is related to the relative abundances of compounds Ib, Ic, 7-methyl
390 brGDGTs and the late-eluting homologs 1050d and 1036d that scored negatively on the first axis
391 of the RDA (Fig. 5a). This is in line with the positive significant correlations between salinity and
392 the relative abundances of these compounds (Fig. S4). This trends also support the assumption
393 made about the aquatic production of ring-containing tetramethylated brGDGTs (Ib and Ic) in
394 Svalbard fjords which was thought to be linked to a salinity change (Dearing Crampton-Flood et

al., 2019). The 7-methyl brGDGTs and their late-eluting isomers, were also shown to be much more abundant in hypersaline lakes than those of lower salinity (Wang et al., 2021). Such a salinity-dependent brGDGT composition has previously been interpreted by membrane adaptation to salinity changes or by a shift in bacterial community composition (Dearing Crampton-Flood et al., 2019; Wang et al., 2021). Hence, the significant positive correlations between salinity and these compounds in the Seine River basin suggest that brGDGT-producing bacteria have similar physiological mechanisms (i.e., membrane adaptation) to those reported in other aquatic settings (lakes and fjords) and/or that the diversity of these bacteria changing along the river-sea continuum.

The relative abundances of several 6-methyl brGDGTs (i.e. IIa_6, $IIIa_6$, and IIb_6) in the Seine River basin reveal significant negative correlations with salinity ($p<0.05$, Wilcoxon test; Fig. S4), which is in contrast with the positive relationships previously found in lakes (Wang et al., 2021). The distinct behavior of 6-methyl brGDGTs between lakes and the Seine river-sea continuum might be due to the lower salinity range in the Seine River basin (0-32 psu) *vs.* the lakes (0-376 psu) investigated by Wang et al. (2021). This suggests that the limited range of salinity variation in the Seine River basin might be insufficient to trigger significant 6-methyl brGDGT production as observed in hypersaline lakes.

Alternatively, the significant negative correlations between the salinity and the relative abundance of 6-methyl brGDGTs in the Seine basin suggest that the bacteria producing 6-methyl brGDGTs are preferentially present in the low salinity area of the estuary. To explore this hypothesis, we investigate the spatio-temporal variations of the 6-methyl *vs*. 5-methyl brGDGTs ratio: IR_{6Me} (Fig. 7). High IR_{6Me} values (0.69 ± 0.10) are associated with enhanced *in situ* production of 6-methyl brGDGTs within the Yenisei river (De Jonge et al., 2015). In the Seine River basin, seasonal variation in IR_{6me} is observed, especially in the upstream part with a low

418 salinity range (0-0.32 psu). Specifically, much higher IR_{6Me} values are observed in the freshwater
419 zone of the estuary (KP 243-297.6; site 7 to site 12) with a low salinity range (0-0.32 psu) during
420 low-flow season (Fig. 7), suggesting that 6-methyl brGDGTs are preferentially produced in this
421 zone when water discharge is low. Similarly, preferential production of 6-methyl brGDGT at low
422 discharges was previously observed in other river systems, including the Amazon River basin
423 (Kirkels et al., 2020; Crampton-Flood et al., 2021; Bertassoli et al., 2022) as well as Black and
424 White Rivers (Dai et al., 2019). It was suggested that the enhanced 6-methyl brGDGT production
425 at low flows was due to slow flow velocity and reduced soil mobilization. Although these
426 hypotheses could account for the temporal variation in IR_{6Me} in the Seine River basin, they are
427 unlikely to explain the substantially high IR_{6Me} values in this specific zone. Other environmental
428 variables such as dissolved oxygen contents (Wu et al., 2021) and pH (De Jonge et al., 2014, 2015)
429 were previously suggested to have a potential influence on 6-methyl brGDGT distributions.
430 Nevertheless, these two environmental factors do not co-vary with IR_{6Me} in the present study and
431 can be ruled out as causes of variation in 6-methyl brGDGT distribution along the Seine river-sea
432 continuum (Fig. 7). Hence, the production of 6-methyl brGDGTs in the upstream zone of the Seine
433 Estuary has to be triggered by other factors, such as the nutrient concentration.

434 High nutrient levels were shown to favor the production of 6-methyl versus 5-methyl
435 brGDGTs in the water column of mesocosm experiments (Martínez-Sosa and Tierney, 2019). As
436 the nutrient concentration is higher in the upstream part of the Seine estuary (Wei et al., 2022), the
437 substantial 6-methyl brGDGT production observed in the aforementioned zone (KP 243-297.6, Fig.
438 7) at low flows could be due to the high amount of nutrients, especially nitrogen. This is supported
439 by the RDA triplot showing strong correlation of TN with the brGDGT distribution in the Seine
440 basin (Fig. 5b), with the major 6-methyl brGDGTs (i.e. IIa_6 and $IIIa_6$) plotting close to TN in the

RDA triplot (Fig. 5a). In addition, TN and $\delta^{15}N$ are observed to co-vary with IR_{6Me} and to peak in the same zone (KP 243-297.6; Fig. 7) during the low-flow season. Nitrate from sewage effluents and manure are generally enriched in ^{15}N compared to other sources, leading to much elevated $\delta^{15}N$ values (10–25‰) (Andrisoa et al., 2019; Leavitt et al., 2006). Nutrients, in the form of nitrogen, can be concentrated at low discharges, thus triggering phytoplankton blooms (Romero et al., 2019). Hence, the elevated TN and $\delta^{15}N$ signals in SPM of the upstream estuary could be attributed to the increase of nitrogen loadings and ^{15}N-enriched nitrate uptake by phytoplankton developing intensively during the low-flow season. The much higher chlorophyll *a* concentrations in the upstream estuary under low discharge conditions support the hypothesis of phytoplankton blooms (Fig. 7). This high phytoplankton biomass might consequently create an environment that accelerates the growth and production of heterotrophic bacteria, which can in turn transform phytoplankton-derived organic matter (Buchan et al., 2014). As the brGDGT-producers were suggested to have a heterotrophic lifestyle (Weijers et al., 2010; Huguet et al., 2017; Blewett et al., 2022), they may transform phytoplankton-derived organic matter and thus participate in N-cycling during blooms. Hence, the co-variations of all the parameters (IR_{6Me}, TN, $\delta^{15}N$, and Chl *a* concentration) peaking in the upstream area during low-flow season suggest that low salinity range and high phytoplankton productivity represent favorable conditions for 6-methyl brGDGT production.

4.2. Sources of brGMGTs and environmental controls on their distribution

4.2.1 Sources of brGMGTs

Similarly to the brGDGTs, the brGMGTs can also be produced *in situ* within the aquatic settings (Baxter et al., 2021; Kirkels et al., 2022a). In previous studies, brGMGTs were detected only in part of the soils surrounding the Godavari River basin (India; Kirkels et al., 2022a) and

464 Lake Chala (East Africa; Baxter et al., 2021), suggesting a limited brGMGT production in soils in
465 comparison to aquatic settings. Consistently, in the Seine River basin, concentrations of brGMGTs
466 in SPM and sediment samples are significantly higher than those in soils ($p<0.05$, Wilcoxon test;
467 Fig. S2b), pointing out their predominant aquatic source.

468 A notable compositional shift in brGMGT distribution is observed along the Seine River
469 basin, as revealed by the separation of riverine, upstream and downstream estuarine samples in the
470 PCA (Fig. 4b). The relative abundance of 3 brGMGTs (H1020c, H1034b, and H1034c) gradually
471 decreases across the basin (Fig. 6) and is significantly correlated with those of 6-methyl brGDGTs
472 (Fig. S5a). As 6-methyl brGDGTs are mainly produced in freshwaters in the Seine basin, this
473 suggests that brGMGTs H1020c, H1034b and H1034c and 6-methyl brGDGTs have a common
474 freshwater origin and that the mixture of fresh and marine waters along the estuary leads to the
475 dilution of these compounds during downstream transport. H1020c is the dominant brGMGT
476 homologue in SPM from the riverine zone of the Seine and one of the most abundant brGMGT in
477 the upstream part of the estuary (Fig. 6). Such a trend was also observed in SPM and riverbed
478 sediments from the upper part of the Godavari River basin, which was attributed to *in situ* riverine
479 brGMGT production of this compound (Kirkels et al., 2022a).

480 The fractional abundance of H1020a and H1020b homologues gradually increases along
481 the Seine River basin. This is consistent with the higher abundances of H1020a and H1020b
482 previously reported in marine sediments from the Bay of Bengal (Kirkels et al., 2022a). The
483 predominance of these compounds in such samples was attributed to their *in situ* production in the
484 marine realm. In line with this hypothesis, the relative abundances of brGMGTs H1020a and
485 H1020b significantly correlate with brGDGTs Ib, Ic, $IIIa_7$, IIa_7 and 1050d (Fig. S5a) in the Seine
486 Estuary, suggesting a similar marine origin.

487 *4.2.2. Environmental controls on the distribution of brGMGTs*

488 The current knowledge on the parameters controlling the brGMGT distributions in the
489 terrestrial and marine realm is still limited. The correlations between the brGDGT and brGMGT
490 relative abundances in the Seine River basin (Fig. S5a) suggest that both types of compounds might
491 be derived from overlapping source microorganisms, with common environmental factors
492 controlling their membrane lipid composition. In the Seine River basin, salinity is shown to be the
493 main environmental parameter influencing the brGMGT distribution, as also observed for
494 brGDGTs (Fig. 5). This is reflected in the significant (p<0.05) increase in the relative abundances
495 of homologues H1020a and H1020b with salinity and a concomitant significant negative
496 correlation between this parameter and the relative abundances of homologues H1020c, H1034b,
497 and H1034c (p<0.05, Wilcoxon test; Fig. 8a). Nevertheless, the individual effect of TN on
498 brGMGT relative abundances is observed to be much lower compared to that observed for
499 brGDGTs (Fig. 5 and Table S2). This implies that, while having common controlling factors such
500 as the salinity, they are also influenced by distinct parameters (i.e. TN), likely indicating distinct
501 sources. This is consistent with a recent study showing that brGDGTs and brGMGTs likely
502 originate from overlapping, but not identical origins (Elling et al., 2023).

503 The shift in brGMGT distribution observed across the Seine River basin (Figs. 5b and 8a)
504 could be due to a change in the diversity of brGMGT-producing bacteria and/or to an adaptation
505 of these microorganisms to environmental changes occurring from upstream to downstream. The
506 latter hypothesis seems unlikely, as a physiological adaptation of a given bacterial community
507 would make it difficult to explain why the relative abundance of three isomers of compound H1020,
508 which share a similar structure, varies differently in response to salinity changes. Hence, a shift in
509 brGMGT-producing bacterial communities across the basin is more likely. Compounds H1020c,

H1034b, and H1034c could predominantly be produced by bacteria preferentially growing in freshwater, and homologues H1020a and H1020b by bacteria preferentially living in brackish or saltwater.

4.3. Potential implications for brGMGTs as a proxy for riverine runoff

The distinct brGMGT distributions in freshwater and saltwater could be used to trace the Organic Matter (OM) produced upstream all along the Seine basin. To trace such a riverine runoff signal, we propose a new proxy, the Riverine IndeX (RIX), based on the fractional abundances of brGMGTs H1020c, H1034c, and H1034b versus H1020a and H1020b (Eq. 3):

$$\mathrm{RIX} = \frac{H1020c+H1034c+H1034b}{H1020c+H1034c+H1034b+H1020a+H1020b} \quad (3)$$

The RIX is calculated for the SPM and sediment samples from the Seine River basin, showing an obvious decreasing trend from upstream to downstream (Fig. 8b). The RIX in river (0.54±0.13, SPM) and upstream estuarine (0.44±0.12, SPM and sediments) samples is significantly higher than for downstream estuarine (0.27±0.12, SPM and sediments) samples. RIX values around 0.50 could therefore be considered reflecting the riverine endmember, while those below 0.30 could represent the saltwater endmember.

As it cannot be completely ruled out that part of the brGMGT signal in the water masses of the Seine may be partially derived from surrounding soils, this index is also calculated for the soil samples. The RIX values of the soil samples are 0.26±0.17, close to those of the downstream estuarine samples. However, the average concentrations of brGMGTs are an order of magnitude lower in the soils than in the sediments and SPM samples of the Seine basin. Therefore, it can be assumed that the impact of soil-derived brGMGTs on the observed RIX signal in the water column of the Seine basin is low.

In order to test the general applicability of the RIX, it was then applied to riverine and marine samples (SPM and sediments) collected in the Godavari River basin and Bay of Bengal (Kirkels et al., 2022a). This site represents the only other river-sea continuum besides the Seine basin for which brGMGT data are presently available. Significant differences in RIX between the SPM and sediment samples from the Godavari River basin are observed (p<0.05, Wilcoxon test; Fig. 8b). In addition, 96% of the RIX values in riverine SPM and riverbed sediments from the Godavari basin exceed 0.5, whereas all of the RIX values observed in marine sediments from the Bay of Bengal are below 0.3. This suggests that the RIX cutoff values defined using the samples from the Seine basin may be broadly applicable and valid across other river-sea continuums. This deserves further studies.

Further confirmation of the RIX potential as a tracer of riverine OM comes from the significant correlations observed between this index and other commonly used proxies for tracing OM sources, i.e. the BIT and $\delta^{13}C_{org}$ (p<0.05, Wilcoxon test; Fig. S5b). These proxies show roughly similar spatial and temporal variations in the Seine River basin. In the low-flow season, RIX and BIT gradually decrease while $\delta^{13}C_{org}$ increase across the basin (Fig. 9). Such trends during the low discharge periods likely reflects the continuous dilution process of riverine OM caused by the mixing of fresh and marine water masses (Thibault et al., 2019). The gradual dilution of the riverine OM signal along the Seine River basin could be due to the increase of seawater intrusion, and thus marine-derived OM, at low discharges (Kolb et al., 2022; Ralston and Geyer, 2019). In contrast, during the high-flow season, no such gradual dilution trend is observed. Instead, at high discharges, the RIX, BIT and $\delta^{13}C_{org}$ remain roughly stable from KP 202 to 310.5, before, steeply decreasing for BIT and RIX, and increasing for $\delta^{13}C_{org}$. This trend can be explained by the fact that at high flow rates, the limit of saltwater intrusion in the estuary shifts seawards rather than landwards,

allowing the riverine OM to be flushed further downstream than under low discharge conditions. After KP 310.5, the riverine OM is diluted because of the mixing with marine water masses, as observed during the low-flow season. The trends observed in the Seine Estuary are consistent with previous studies in other regions, showing that terrestrial OM was only effectively transported downstream at high flow rates (Kirkels et al., 2022b, 2020).

Although the BIT is successfully used in the Seine River basin as well as in previous studies to trace riverine (terrestrial) OM inputs (Hopmans et al., 2004; Xu et al., 2020), this index can be biased by *in situ* production of brGDGTs in aquatic settings (Dearing Crampton-Flood et al., 2019; Sinninghe Damsté, 2016) and selective degradation of crenarchaeol *vs.* brGDGTs (Smith et al., 2012). Hence, high BIT values do not necessarily indicate higher contribution of terrestrial OM in some settings (Smith et al., 2012). Unlike the BIT index, based on two different families of compounds (isoGDGTs and brGDGTs), the RIX is based on 5 compounds from the same family (brGMGTs) that likely have similar degradation rates and therefore not influenced by selective degradation. Furthermore, the RIX is based on the relative abundances of brGMGTs which are all predominantly produced in aquatic settings, three of them (H1020c, H1034b, and H1034c) being mainly produced in freshwater and two of them (H1020a and H1020b) mainly in saltwater. Therefore, the RIX is based on compounds which are more specifically produced in the two endmembers (freshwater or saltwater), which could avoid the biases encountered with the BIT. Overall, our work shows that, in addition to the BIT and $\delta^{13}C_{org}$, the RIX successfully captures the spatio-temporal dynamics of riverine OM in the Seine River basin, making this proxy a promising and complementary one tracing riverine runoff in modern samples as well as paleorecords.

5. Conclusions

In this study, the brGDGT and brGMGT concentrations and distributions in soils, SPM, and sediments (n=237) across the Seine River basin were investigated. Higher concentrations and distinct distributions of brGDGTs and brGMGTs in SPM and sediments compared with soils imply that both types of compounds can be produced *in situ* in aquatic settings. The distribution of both brGDGTs and brGMGTs are largely related to salinity, but only brGDGT distributions are significantly influenced by nitrogen nutrient loadings. In addition, covariations of IR_{6Me}, TN, $\delta^{15}N$, and Chl *a* concentration within the low salinity region suggest that riverine (6-methyl) brGDGT production is favored by low-salinity and high-productivity conditions.

In the Seine River basin, salinity correlate positively with H1020a and H1020b, and negatively with H1020c, H1034b, and H1034c. This indicates that compounds H1020c, H1034b, and H1034c could be produced by bacteria that preferentially grow in freshwater, while homologues H1020a and H1020b could be produced by bacteria that mainly live in saltwater. Based on this, a novel proxy, the Riverine IndeX (RIX) is proposed to trace riverine OM input. The average value of RIX for the riverine samples is 0.54, which is much higher than that in soils (0.26 on average) and downstream estuarine (0.27 on average) samples. We thus recommend that RIX values over 0.5 imply considerable riverine contributions, whereas RIX values below 0.3 indicate higher marine contributions. This cutoff value defined in the Seine River basin also works in the Godavari River basin (India), which implies that this novel proxy based on brGMGTs may be broadly applicable and warrants further exploration.

Acknowledgments

We would like to thank members of the SARTRE project for their assistance during the field campaigns. We appreciate the logistical support from Robert Lafite, Frédéric Azémar, Anaëlle Bernard and Mahaut Sourzac. We are grateful to Pascal Claquin and Léo Chasselin for their support in water quality measurements and Micky Tackx for the scientific coordination of the SARTRE project. This study was funded by GIP Seine-Aval (MOSAIC, PHARESEE, FEREE and SARTRE projects) and CNRS/INSU and OFB (EC2CO RUNTIME project). Zhe-Xuan Zhang's PhD scholarship is funded by China Scholarship Council (No. 202004910406) and ASDB from Sorbonne Université. This work was supported by CESAM (UIDP/50017/2020 + UIDB/50017/2020 + LA/P/0094/2020).

Appendix A. Supplementary material

The brGDGT and brGMGT data are made available in the Supplementary material and will be archived in PANGAEA by the time of publication.

References

Andrisoa, A., Stieglitz, T.C., Rodellas, V., Raimbault, P., 2019. Primary production in coastal lagoons supported by groundwater discharge and porewater fluxes inferred from nitrogen and carbon isotope signatures. Mar. Chem. 210, 48–60.

Baxter, A.J., Hopmans, E.C., Russell, J.M., Sinninghe Damsté, J.S., 2019. Bacterial GMGTs in East African lake sediments: Their potential as palaeotemperature indicators. Geochim. Cosmochim. Acta 259, 155–169.

Baxter, A.J., Peterse, F., Verschuren, D., Sinninghe Damsté, J.S., 2021. Anoxic in situ production of bacterial GMGTs in the water column and surficial bottom sediments of a meromictic tropical crater lake: Implications for lake paleothermometry. Geochim. Cosmochim. Acta 306, 171–188.

Bertassoli, D.J., Häggi, C., Chiessi, C.M., Schefuß, E., Hefter, J., Akabane, T.K., Sawakuchi, A.O., 2022. Controls on the distributions of GDGTs and n-alkane isotopic compositions in sediments of the Amazon River Basin. Chem. Geol. 594, 120777.

Bijl, P.K., Frieling, J., Cramwinckel, M.J., Boschman, C., Sluijs, A., Peterse, F., 2021. Maastrichtian–Rupelian paleoclimates in the southwest Pacific – a critical re-evaluation of biomarker paleothermometry and dinoflagellate cyst paleoecology at Ocean Drilling Program Site 1172. Clim. Past 17, 2393–2425.

Blewett, J., Elling, F.J., Naafs, B.D.A., Kattein, L., Evans, T.W., Lauretano, V., Gallego-Sala, A.V., Pancost, R.D., Pearson, A., 2022. Metabolic and ecological controls on the stable carbon isotopic composition of archaeal (isoGDGT and BDGT) and bacterial (brGDGT) lipids in wetlands and lignites. Geochim. Cosmochim. Acta 320, 1–25.

Buchan, A., LeCleir, G.R., Gulvik, C.A., González, J.M., 2014. Master recyclers: features and functions of bacteria associated with phytoplankton blooms. Nat. Rev. Microbiol. 12, 686–698.

Cao, J., Lian, E., Yang, S., Ge, H., Jin, X., He, J., Jia, G., 2022. The distribution of intact polar lipid-derived branched tetraethers along a freshwater-seawater pH gradient in coastal East China Sea. Chem. Geol. 596, 120808.

Chen, Y., Zheng, F., Yang, H., Yang, W., Wu, R., Liu, X., Liang, H., Chen, H., Pei, H., Zhang, C., Pancost, R.D., Zeng, Z., 2022. The production of diverse brGDGTs by an Acidobacterium providing a physiological basis for paleoclimate proxies. Geochim. Cosmochim. Acta.

Coffinet, S., Huguet, A., Bergonzini, L., Pedentchouk, N., Williamson, D., Anquetil, C., Gałka, M., Kołaczek, P., Karpińska-Kołaczek, M., Majule, A., Laggoun-Défarge, F., Wagner, T., Derenne, S., 2018. Impact of climate change on the ecology of the Kyambangunguru crater marsh in southwestern Tanzania during the Late Holocene. Quat. Sci. Rev. 196, 100–117.

Crampton-Flood, E.D., van der Weijst, C.M., van der Molen, G., Bouquet, M., Yedema, Y., Donders, T.H., Sangiorgi, F., Sluijs, A., Damsté, J.S.S., Peterse, F., 2021. Identifying marine and freshwater overprints on soil-derived branched GDGT temperature signals in Pliocene Mississippi and Amazon River fan sediments. Org. Geochem. 154, 104200.

Cramwinckel, M.J., Huber, M., Kocken, I.J., Agnini, C., Bijl, P.K., Bohaty, S.M., Frieling, J., Goldner, A., Hilgen, F.J., Kip, E.L., Peterse, F., van der Ploeg, R., Röhl, U., Schouten, S., Sluijs, A., 2018. Synchronous tropical and polar temperature evolution in the Eocene. Nature 559, 382–386.

Dai, G., Zhu, E., Liu, Z., Wang, Y., Zhu, S., Wang, S., Ma, T., Jia, J., Wang, X., Hou, S., Fu, P., Peterse, F., Feng, X., 2019. Compositional Characteristics of Fluvial Particulate Organic Matter Exported From the World's Largest Alpine Wetland. J. Geophys. Res. Biogeosciences 124, 2709–2727.

De Jonge, C., Hopmans, E.C., Stadnitskaia, A., Rijpstra, W.I.C., Hofland, R., Tegelaar, E., Sinninghe Damsté, J.S., 2013. Identification of novel penta- and hexamethylated branched glycerol dialkyl glycerol tetraethers in peat using HPLC–MS2, GC–MS and GC–SMB-MS. Org. Geochem. 54, 78–82.

De Jonge, C., Hopmans, E.C., Zell, C.I., Kim, J.-H., Schouten, S., Sinninghe Damsté, J.S., 2014. Occurrence and abundance of 6-methyl branched glycerol dialkyl glycerol tetraethers in soils: Implications for palaeoclimate reconstruction. Geochim. Cosmochim. Acta 141, 97–112.

De Jonge, C., Stadnitskaia, A., Hopmans, E.C., Cherkashov, G., Fedotov, A., Streletskaya, I.D., Vasiliev, A.A., Sinninghe Damsté, J.S., 2015. Drastic changes in the distribution of branched tetraether lipids in suspended matter and sediments from the Yenisei River and

673 Kara Sea (Siberia): Implications for the use of brGDGT-based proxies in coastal marine
674 sediments. Geochim. Cosmochim. Acta 165, 200–225.
675 Dearing Crampton-Flood, E., Peterse, F., Sinninghe Damsté, J.S., 2019. Production of branched
676 tetraethers in the marine realm: Svalbard fjord sediments revisited. Org. Geochem. 138,
677 103907.
678 Ding, S., Schwab, V.F., Ueberschaar, N., Roth, V.-N., Lange, M., Xu, Y., Gleixner, G., Pohnert,
679 G., 2016. Identification of novel 7-methyl and cyclopentanyl branched glycerol dialkyl
680 glycerol tetraethers in lake sediments. Org. Geochem. 102, 52–58.
681 Elling, F.J., Kattein, L., David A. Naafs, B., Lauretano, V., Pearson, A., 2023. Heterotrophic origin
682 and diverse sources of branched glycerol monoalkyl glycerol tetraethers (brGMGTs) in
683 peats and lignites. Org. Geochem. 104558.
684 Flipo, N., Lestel, L., Labadie, P., Meybeck, M., Garnier, J., 2021. Trajectories of the Seine River
685 Basin, in: Flipo, N., Labadie, P., Lestel, L. (Eds.), The Seine River Basin, The Handbook
686 of Environmental Chemistry. Springer International Publishing, Cham, pp. 1–28.
687 Halamka, T.A., Raberg, J.H., McFarlin, J.M., Younkin, A.D., Mulligan, C., Liu, X.-L., Kopf, S.H.,
688 2022. Production of diverse brGDGTs by Acidobacterium Solibacter usitatus in response
689 to temperature, pH, and O2 provides a culturing perspective on brGDGT proxies and
690 biosynthesis. Geobiology.
691 Harning, D.J., Curtin, L., Geirsdóttir, Á., D'Andrea, W.J., Miller, G.H., Sepúlveda, J., 2020. Lipid
692 Biomarkers Quantify Holocene Summer Temperature and Ice Cap Sensitivity in Icelandic
693 Lakes. Geophys. Res. Lett. 47, e2019GL085728.
694 Hopmans, E.C., Schouten, S., Sinninghe Damsté, J.S., 2016. The effect of improved
695 chromatography on GDGT-based palaeoproxies. Org. Geochem. 93, 1–6.
696 Hopmans, E.C., Weijers, J.W.H., Schefuß, E., Herfort, L., Sinninghe Damsté, J.S., Schouten, S.,
697 2004. A novel proxy for terrestrial organic matter in sediments based on branched and
698 isoprenoid tetraether lipids. Earth Planet. Sci. Lett. 224, 107–116.
699 Huguet, A., Coffinet, S., Roussel, A., Gayraud, F., Anquetil, C., Bergonzini, L., Bonanomi, G.,
700 Williamson, D., Majule, A., Derenne, S., 2019. Evaluation of 3-hydroxy fatty acids as a pH
701 and temperature proxy in soils from temperate and tropical altitudinal gradients. Org.
702 Geochem. 129, 1–13.
703 Huguet, A., Meador, T.B., Laggoun-Défarge, F., Könneke, M., Wu, W., Derenne, S., Hinrichs, K.-
704 U., 2017. Production rates of bacterial tetraether lipids and fatty acids in peatland under
705 varying oxygen concentrations. Geochim. Cosmochim. Acta 203, 103–116.
706 Huguet, C., Hopmans, E.C., Febo-Ayala, W., Thompson, D.H., Sinninghe Damsté, J.S., Schouten,
707 S., 2006. An improved method to determine the absolute abundance of glycerol
708 dibiphytanyl glycerol tetraether lipids. Org. Geochem. 37, 1036–1041.
709 Kirkels, F.M.S.A., Ponton, C., Galy, V., West, A.J., Feakins, S.J., Peterse, F., 2020. From Andes
710 to Amazon: Assessing Branched Tetraether Lipids as Tracers for Soil Organic Carbon in
711 the Madre de Dios River System. J. Geophys. Res. Biogeosciences 125, e2019JG005270.
712 Kirkels, F.M.S.A., Usman, M.O., Peterse, F., 2022a. Distinct sources of bacterial branched GMGTs
713 in the Godavari River basin (India) and Bay of Bengal sediments. Org. Geochem. 167,
714 104405.
715 Kirkels, F.M.S.A., Zwart, H.M., Usman, M.O., Hou, S., Ponton, C., Giosan, L., Eglinton, T.I.,
716 Peterse, F., 2022b. From soil to sea: sources and transport of organic carbon traced by
717 tetraether lipids in the monsoonal Godavari River, India. Biogeosciences 19, 3979–4010.

718 Kolb, P., Zorndt, A., Burchard, H., Gräwe, U., Kösters, F., 2022. Modelling the impact of
719 anthropogenic measures on saltwater intrusion in the Weser estuary. Ocean Sci. 18, 1725–
720 1739.
721 Kou, Q., Zhu, L., Ju, J., Wang, J., Xu, T., Li, C., Ma, Q., 2022. Influence of salinity on glycerol
722 dialkyl glycerol tetraether-based indicators in Tibetan Plateau lakes: Implications for
723 paleotemperature and paleosalinity reconstructions. Palaeogeogr. Palaeoclimatol.
724 Palaeoecol. 601, 111127.
725 Lai, J., Zou, Y., Zhang, J., Peres-Neto, P.R., 2022. Generalizing hierarchical and variation
726 partitioning in multiple regression and canonical analyses using the rdacca.hp R package.
727 Methods Ecol. Evol. 13, 782–788.
728 Leavitt, P.R., Brock, C.S., Ebel, C., Patoine, A., 2006. Landscape-scale effects of urban nitrogen
729 on a chain of freshwater lakes in central North America. Limnol. Oceanogr. 51, 2262–2277.
730 Liu, X.-L., Summons, R.E., Hinrichs, K.-U., 2012. Extending the known range of glycerol ether
731 lipids in the environment: structural assignments based on tandem mass spectral
732 fragmentation patterns. Rapid Commun. Mass Spectrom. 26, 2295–2302.
733 Martínez-Sosa, P., Tierney, J.E., 2019. Lacustrine brGDGT response to microcosm and mesocosm
734 incubations. Org. Geochem. 127, 12–22.
735 Martínez-Sosa, P., Tierney, J.E., Stefanescu, I.C., Dearing Crampton-Flood, E., Shuman, B.N.,
736 Routson, C., 2021. A global Bayesian temperature calibration for lacustrine brGDGTs.
737 Geochim. Cosmochim. Acta 305, 87–105.
738 Naafs, B.D.A., Inglis, G.N., Zheng, Y., Amesbury, M.J., Biester, H., Bindler, R., Blewett, J.,
739 Burrows, M.A., del Castillo Torres, D., Chambers, F.M., Cohen, A.D., Evershed, R.P.,
740 Feakins, S.J., Gałka, M., Gallego-Sala, A., Gandois, L., Gray, D.M., Hatcher, P.G., Honorio
741 Coronado, E.N., Hughes, P.D.M., Huguet, A., Könönen, M., Laggoun-Défarge, F.,
742 Lähteenoja, O., Lamentowicz, M., Marchant, R., McClymont, E., Pontevedra-Pombal, X.,
743 Ponton, C., Pourmand, A., Rizzuti, A.M., Rochefort, L., Schellekens, J., De Vleeschouwer,
744 F., Pancost, R.D., 2017. Introducing global peat-specific temperature and pH calibrations
745 based on brGDGT bacterial lipids. Geochim. Cosmochim. Acta 208, 285–301.
746 Naafs, B.D.A., McCormick, D., Inglis, G.N., Pancost, R.D., 2018. Archaeal and bacterial H-
747 GDGTs are abundant in peat and their relative abundance is positively correlated with
748 temperature. Geochim. Cosmochim. Acta 227, 156–170.
749 Peterse, F., Kim, J.-H., Schouten, S., Kristensen, D.K., Koç, N., Sinninghe Damsté, J.S., 2009.
750 Constraints on the application of the MBT/CBT palaeothermometer at high latitude
751 environments (Svalbard, Norway). Org. Geochem. 40, 692–699.
752 Raberg, J.H., Miller, G.H., Geirsdóttir, Á., Sepúlveda, J., 2022. Near-universal trends in brGDGT
753 lipid distributions in nature. Sci. Adv. 8, eabm7625.
754 Ralston, D.K., Geyer, W.R., 2019. Response to Channel Deepening of the Salinity Intrusion,
755 Estuarine Circulation, and Stratification in an Urbanized Estuary. J. Geophys. Res. Oceans
756 124, 4784–4802.
757 Romero, E., Garnier, J., Billen, G., Ramarson, A., Riou, P., Le Gendre, R., 2019. Modeling the
758 biogeochemical functioning of the Seine estuary and its coastal zone: Export, retention, and
759 transformations. Limnol. Oceanogr. 64, 895–912.
760 Ryba, S.A., Burgess, R.M., 2002. Effects of sample preparation on the measurement of organic
761 carbon, hydrogen, nitrogen, sulfur, and oxygen concentrations in marine sediments.
762 Chemosphere 48, 139–147.
763 Schouten, S., Hopmans, E.C., Sinninghe Damsté, J.S., 2013. The organic geochemistry of glycerol
764 dialkyl glycerol tetraether lipids: A review. Org. Geochem. 54, 19–61.

765 Sinninghe Damsté, J.S., 2016. Spatial heterogeneity of sources of branched tetraethers in shelf
766 systems: The geochemistry of tetraethers in the Berau River delta (Kalimantan, Indonesia).
767 Geochim. Cosmochim. Acta 186, 13–31.
768 Sinninghe Damsté, J.S., Rijpstra, W.I.C., Hopmans, E.C., Weijers, J.W.H., Foesel, B.U.,
769 Overmann, J., Dedysh, S.N., 2011. 13,16-Dimethyl octacosanedioic acid (iso-diabolic acid),
770 a common membrane-spanning lipid of Acidobacteria subdivisions 1 and 3. Appl. Environ.
771 Microbiol. 77, 4147–4154.
772 Sluijs, A., Frieling, J., Inglis, G.N., Nierop, K.G.J., Peterse, F., Sangiorgi, F., Schouten, S., 2020.
773 Late Paleocene–early Eocene Arctic Ocean sea surface temperatures: reassessing
774 biomarker paleothermometry at Lomonosov Ridge. Clim. Past 16, 2381–2400.
775 Smith, R.W., Bianchi, T.S., Li, X., 2012. A re-evaluation of the use of branched GDGTs as
776 terrestrial biomarkers: Implications for the BIT Index. Geochim. Cosmochim. Acta 80, 14–
777 29.
778 Strickland, J.D.H., Parsons, T.R., 1972. A Practical Handbook of Seawater Analysis, 2nd edition.
779 Thibault, A., 2018. Dynamique de la matière organique dans la Seine : approche globale et
780 moléculaire (phdthesis). Sorbonne Université.
781 Thibault, A., Derenne, S., Parlanti, E., Anquetil, C., Sourzac, M., Budzinski, H., Fuster, L.,
782 Laverman, A., Roose-Amsaleg, C., Viollier, E., Huguet, A., 2019. Dynamics of organic
783 matter in the Seine Estuary (France): Bulk and structural approaches. Mar. Chem. 212, 108–
784 119.
785 Tierney, J.E., Russell, J.M., 2009. Distributions of branched GDGTs in a tropical lake system:
786 Implications for lacustrine application of the MBT/CBT paleoproxy. Org. Geochem. 40,
787 1032–1036.
788 Véquaud, P., Thibault, A., Derenne, S., Anquetil, C., Collin, S., Contreras, S., Nottingham, A.T.,
789 Sabatier, P., Werne, J.P., Huguet, A., 2022. FROG: A global machine-learning temperature
790 calibration for branched GDGTs in soils and peats. Geochim. Cosmochim. Acta 318, 468–
791 494.
792 Wang, H., An, Z., Lu, H., Zhao, Z., Liu, W., 2020. Calibrating bacterial tetraether distributions
793 towards in situ soil temperature and application to a loess-paleosol sequence. Quat. Sci.
794 Rev. 231, 106172.
795 Wang, H., Liu, W., He, Y., Zhou, A., Zhao, H., Liu, H., Cao, Y., Hu, J., Meng, B., Jiang, J.,
796 Kolpakova, M., Krivonogov, S., Liu, Z., 2021. Salinity-controlled isomerization of
797 lacustrine brGDGTs impacts the associated MBT5ME' terrestrial temperature index.
798 Geochim. Cosmochim. Acta 305, 33–48.
799 Wei, X., Garnier, J., Thieu, V., Passy, P., Le Gendre, R., Billen, G., Akopian, M., Laruelle, G.G.,
800 2022. Nutrient transport and transformation in macrotidal estuaries of the French Atlantic
801 coast: a modeling approach using the Carbon-Generic Estuarine Model. Biogeosciences 19,
802 931–955.
803 Weijers, J.W.H., Schouten, S., van den Donker, J.C., Hopmans, E.C., Sinninghe Damsté, J.S., 2007.
804 Environmental controls on bacterial tetraether membrane lipid distribution in soils.
805 Geochim. Cosmochim. Acta 71, 703–713.
806 Weijers, J.W.H., Wiesenberg, G.L.B., Bol, R., Hopmans, E.C., Pancost, R.D., 2010. Carbon
807 isotopic composition of branched tetraether membrane lipids in soils suggest a rapid
808 turnover and a heterotrophic life style of their source organism(s). Biogeosciences 7, 2959–
809 2973.
810 Wu, J., Yang, H., Pancost, R.D., Naafs, B.D.A., Qian, S., Dang, X., Sun, H., Pei, H., Wang, R.,
811 Zhao, S., Xie, S., 2021. Variations in dissolved O2 in a Chinese lake drive changes in

microbial communities and impact sedimentary GDGT distributions. Chem. Geol. 579, 120348.
Xu, S., Zhang, Z., Jia, G., Yu, K., Lei, F., Zhu, X., 2020. Controlling factors and environmental significance of BIT and δ13C of sedimentary GDGTs from the Pearl River Estuary, China over recent decades. Estuar. Coast. Shelf Sci. 233, 106534.
Yedema, Y.W., Sangiorgi, F., Sluijs, A., Sinninghe Damsté, J.S., Peterse, F., 2023. The dispersal of fluvially discharged and marine, shelf-produced particulate organic matter in the northern Gulf of Mexico. Biogeosciences 20, 663–686.
Zell, C., Kim, J.-H., Balsinha, M., Dorhout, D., Fernandes, C., Baas, M., Sinninghe Damsté, J.S., 2014. Transport of branched tetraether lipids from the Tagus River basin to the coastal ocean of the Portuguese margin: consequences for the interpretation of the MBT'/CBT paleothermometer. Biogeosciences 11, 5637–5655.
Zhang, Z.-X., Li, J., Chen, Z., Sun, Z., Yang, H., Fu, M., Peng, X., 2020. The effect of methane seeps on the bacterial tetraether lipid distributions at the Okinawa Trough. Mar. Chem. 225, 103845.

Captions to figures and tables

Table 1. Location of the sampling sites along the Seine Basin, with the type of samples collected.

Fig. 1. (a) Geographical locations of sampling sites in the Seine River Basin (KP: kilometric point, the distance in kilometers from the city of Paris (KP 0)). (b) Mean monthly water discharge for the Seine River at the Paris Austerlitz station from 2015 to 2021 (data from https://www.hydro.eaufrance.fr/). Bullets represent the sampling period in high-flow (>250 m^3/s - blue) and low-flow (<250 m^3/s - red) seasons.

Fig. 2. Extracted chromatograms of brGDGTs and brGMGTs for the SPM samples collected in (a) site 3 (Triel sur Seine, November 2020), (b) site 10 (Val-des-Leux, July 2019) and (c) site 18 (Honfleur, April 2015). The nomenclature for the penta- and hexamethylated brGDGTs: 5-methyl brGDGTs ($IIIa_5$, $IIIb_5$, $IIIc_5$, IIa_5, IIb_5, and IIc_5); 6-methyl brGDGTs ($IIIa_6$, $IIIb_6$, $IIIc_6$, IIa_6, IIb_6, and IIc_6); 7-methyl brGDGTs ($IIIa_7$, $IIIb_7$, and IIa_7).

Fig. 3. Relative abundances of selected individual brGDGTs from soils (surficial soils and mudflat soils/sediments, *n*=51), river (*n*=9), upstream estuary (*n*=56), and downstream estuary (*n*=121) samples across the Seine River basin: cyclopentane-containing tetramethylated brGDGTs (Ib and Ic), 6-methyl brGDGTs (IIa_6 and $IIIa_6$), 7-methyl brGDGTs (IIa_7 and $IIIa_7$) and brGDGTs 1050d and 1036d. Box plots of upstream and downstream estuary samples are based on SPM and sediments, whereas those of river samples are based only on SPM. Boxes are color-coded based on the sample type (soil in brown, river in red, upstream estuary in yellow, and downstream estuary in blue). Statistical testing was performed by a Wilcoxon test (*P < 0.05; **P < 0.01; ***P < 0.001; ****P < 0.0001; ns, not significant, P >0.05).

Fig. 4. PCA analysis of fractional abundances of (a) brGDGTs and (b) brGMGTs. The dataset used for PCA analysis is composed of SPM and sediments. Adonis analysis was used to evaluate how variation can be explained by the variables (999 permutations).

Fig. 5. RDA analysis showing relationships between environmental factors (TN, TOC, salinity, temperature, purple arrows) and fractional abundances of (a) brGDGTs and (c) brGMGTs. The individual importance of the environmental factors (TN, TOC, salinity, temperature) explaining the variation in (b) brGDGT and (d) brGMGT distributions was determined by hierarchical partitioning analysis. The dataset used for RDA analysis is composed of SPM from river (*n*=6; red), upstream estuary (*n*=42; yellow), and downstream estuary (*n*=59; blue). Significance level is indicated by asterisks: *P < 0.05; **P < 0.01; ***P < 0.001.

Fig. 6. Relative abundance of distinct brGMGTs from soils (surficial soils and mudflat soils/sediments, *n*=51), river (*n*=9), upstream estuary (*n*=56) and downstream estuary (*n*=121) across the Seine River basin. Box plots of upstream and downstream estuary are composed of SPM and sediments, whereas those of river are composed of SPM. Boxes are color-coded based on the sample type (soil in brown, river in red, upstream estuary in yellow, and downstream estuary in blue). Statistical testing was performed by a Wilcoxon test (*P < 0.05; **P < 0.01; ***P < 0.001; ****P < 0.0001; ns, not significant, P >0.05).

Fig. 7. Spatio-temporal variations of IR_{6Me} and several environmental factors, including TN (%), $\delta^{15}N$ (‰), Chla (µg/L), TOC (%), turbidity (NTU), pH, and dissolved oxygen saturation (DO, %). The trends showing variations were based on locally estimated scatterplot smoothing (LOESS) method with 95% confidence intervals. KP (kilometric point) represents the distance in kilometers from the city of Paris (KP 0). Dataset is composed of SPM. The shaded area highlights a zone (KP 243-297.6) where IR_{6Me} and several environmental parameters co-vary.

Fig. 8. (a) Salinity plotted versus relative abundance of brGMGTs. Shaded area represent 95% confidence intervals. Vertical error bars indicate mean ± s.d for samples with the same salinity. Dataset is composed of SPM. (b) Distribution of RIX across the Seine River basin. Boxes are color-coded based on the sample type (river in red, upstream estuary in yellow, and downstream estuary in blue). Dataset is composed of SPM and sediments. (c) RIX in the Godavari River basin (India) and Bay of Bengal sediments (data from Kirkels et al. (2022a)). Statistical testing was performed by a Wilcoxon test.

Fig. 9. Spatio-temporal variations of RIX and several other terrestrial proxies, including BIT and $\delta^{13}C$ (‰). The trends showing spatio-temporal variations were based on locally estimated scatterplot smoothing (LOESS) method with 95% confidence intervals. KP (kilometric point) represents the distance in kilometers from the city of Paris (KP 0). Dataset is composed of SPM.

909 **Table 1.** Location of the sampling sites along the Seine Basin, with the type of samples collected

Site	Name	Longitude (°)	Latitude (°)	KP	Zone	Date	Type
1	Marnay sur Seine	3.56	48.51	-200	River	2020-11	SPM
2	Bougival	2.13	48.87	40	River	2020-11	SPM
3	Triel sur Seine	2.00	48.98	80	River	2020-11	SPM
4	Les Andelys	1.40	49.24	175	River	2019-6; 2019-7; 2020-9	SPM
5	Poses	1.24	49.31	202	Upstream estuary	2016-4; 2020-11	SPM
6	Oissel	1.10	49.34	229.4	Upstream estuary	2019-6; 2019-7; 2020-9	SPM
7	Rouen	1.03	49.43	243	Upstream estuary	2016-4	SPM; Sediments
8	Petit Couronne	1.01	49.38	251.3	Upstream estuary	2020-9; 2021-2; 2021-3	SPM
9	Grand-Couronne	0.98	49.36	255.6	Upstream estuary	2019-6	SPM
10	Val des Leux	0.92	49.40	265.55	Upstream estuary	2019-6; 2019-7; 2020-9	SPM
11	Duclair	0.87	49.48	278	Upstream estuary	2020-9; 2021-2; 2021-3	SPM
12	Heurtauville	0.82	49.45	297.65	Downstream estuary	2019-6	SPM
13	Caudebec	0.75	49.52	310.5	Downstream estuary	2015-4; 2015-9; 2016-4; 2019-6; 2019-7; 2020-9; 2021-2; 2021-3	SPM; Sediments
14	Vatteville-La-Rue	0.67	49.47	318	Downstream estuary	2019-6	SPM
15	Tancarville	0.47	49.47	337	Downstream estuary	2015-1; 2015-4; 2015-9; 2019-6; 2019-7; 2020-9; 2021-2; 2021-3	SPM; Sediments
16	Berville-Sur-Mer	0.37	49.44	346	Downstream estuary	2019-6	SPM
17	Fatouville	0.32	49.44	350	Downstream estuary	2015-4; 2015-7; 2015-9; 2016-4	SPM; Sediments

18	Honfleur	0.23	49.43	355.8	Downstream estuary	2015-4; 2015-9; 2019-6; 2020-9; 2021-2; 2021-3	SPM
19	La Carosse	0.03	49.48	370	Downstream estuary	2015-7; 2016-4; 2016-4	SPM; Sediments

910

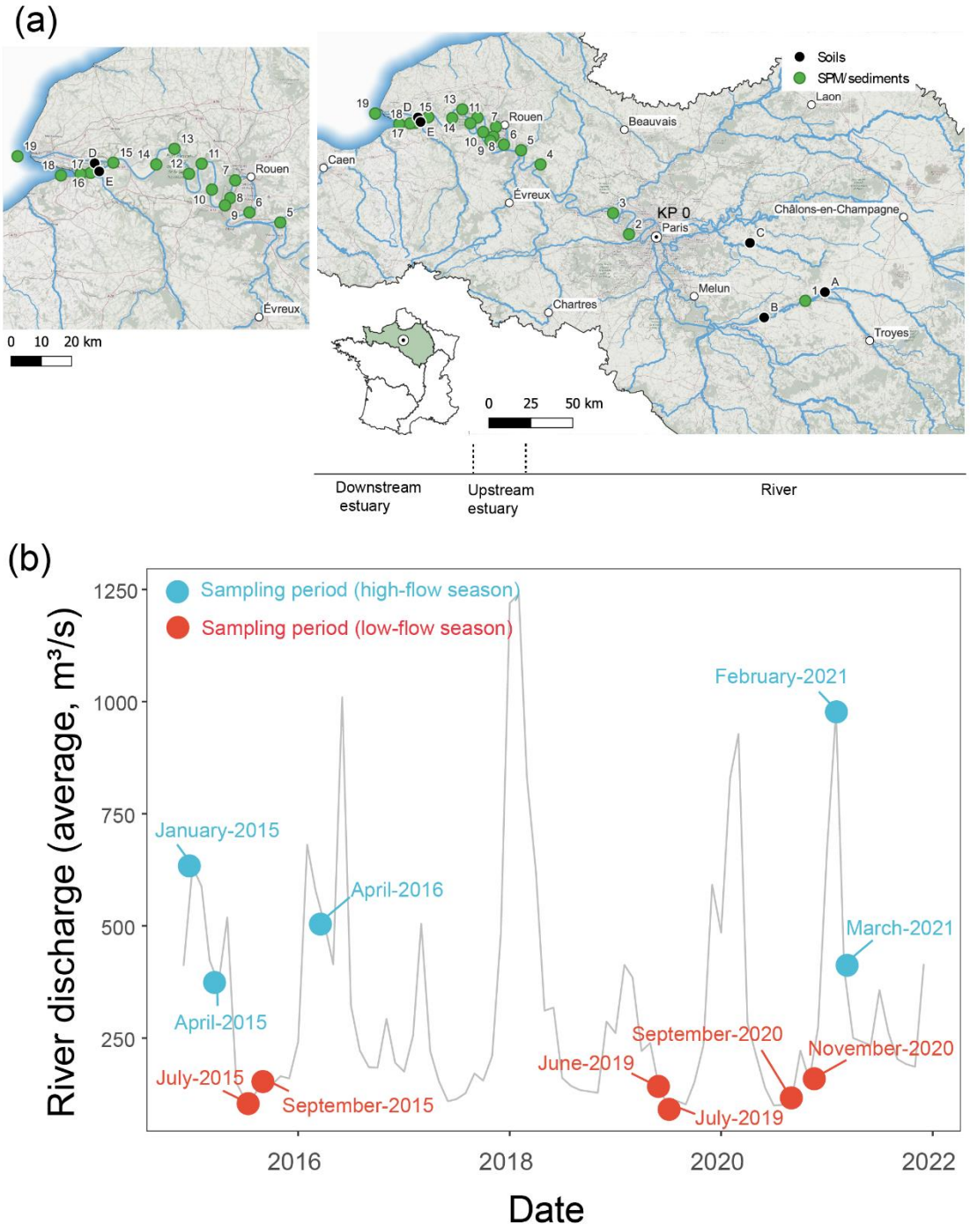

Fig. 1. (a) Geographical locations of sampling sites in the Seine River Basin (KP: kilometric point, the distance in kilometers from the city of Paris (KP 0)). (b) Mean monthly water discharge for the Seine River at the Paris Austerlitz station from 2015 to 2021 (data from https://www.hydro.eaufrance.fr/). Bullets represent the sampling period in high-flow (>250 m^3/s - blue) and low-flow (<250 m^3/s - red) seasons.

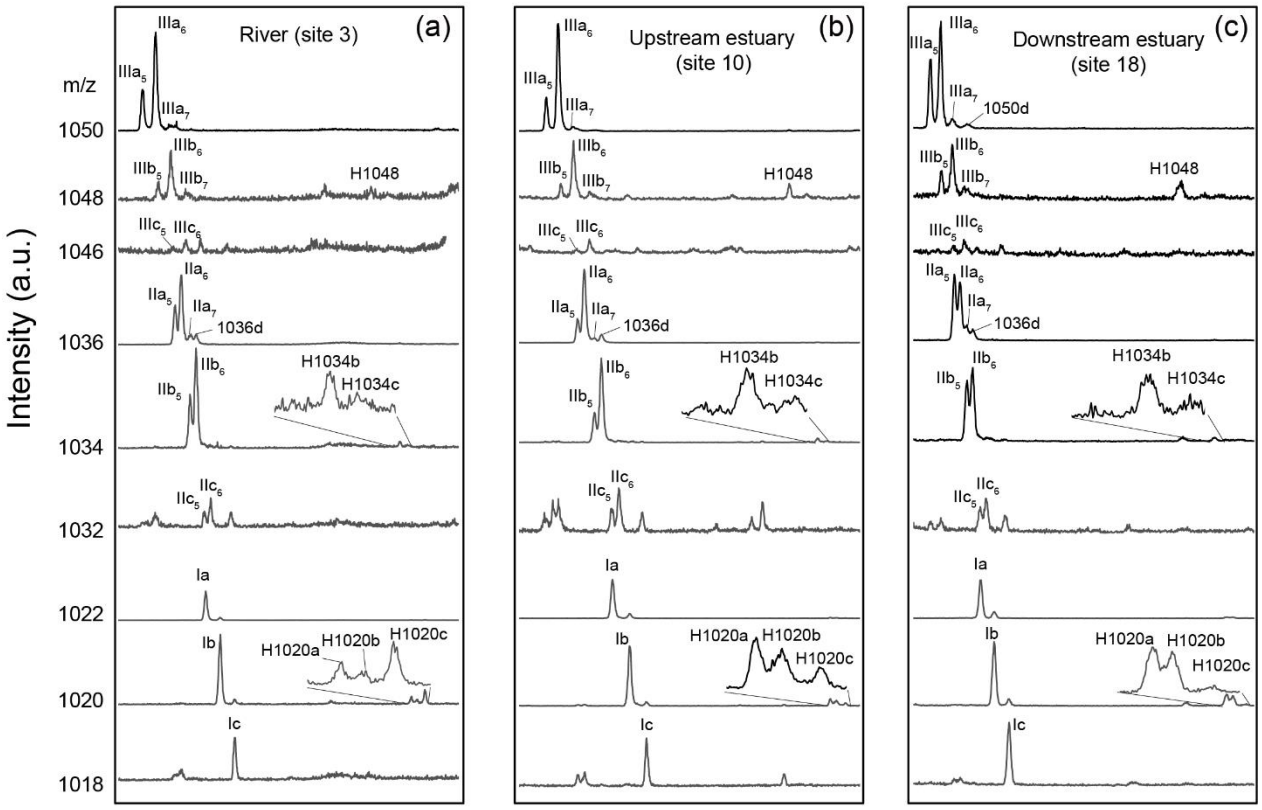

Fig. 2. Extracted chromatograms of brGDGTs and brGMGTs for the SPM samples collected in (a) site 3 (Triel sur Seine, November 2020), (b) site 10 (Val-des-Leux, July 2019) and (c) site 18 (Honfleur, April 2015). The nomenclature for the penta- and hexamethylated brGDGTs: 5-methyl brGDGTs ($IIIa_5$, $IIIb_5$, $IIIc_5$, IIa_5, IIb_5, and IIc_5); 6-methyl brGDGTs ($IIIa_6$, $IIIb_6$, $IIIc_6$, IIa_6, IIb_6, and IIc_6); 7-methyl brGDGTs ($IIIa_7$, $IIIb_7$, and IIa_7).

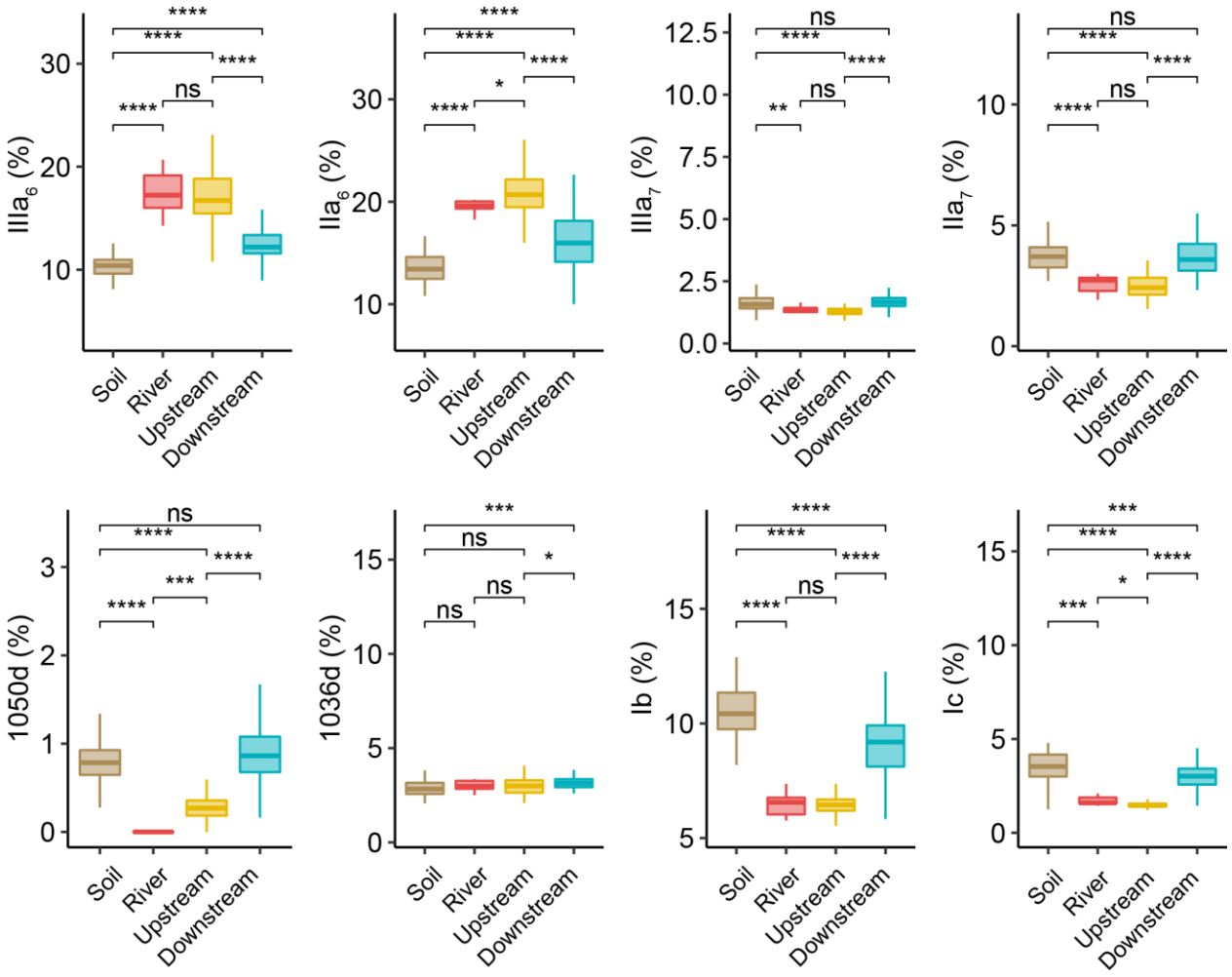

924

925 **Fig. 3.** Relative abundances of selected individual brGDGTs from soils (surficial soils and mudflat
926 soils/sediments, *n*=51), river (*n*=9), upstream estuary (*n*=56), and downstream estuary (*n*=121)
927 samples across the Seine River basin: cyclopentane-containing tetramethylated brGDGTs (Ib and
928 Ic), 6-methyl brGDGTs (IIa_6 and $IIIa_6$), 7-methyl brGDGTs (IIa_7 and $IIIa_7$) and brGDGTs 1050d
929 and 1036d. Box plots of upstream and downstream estuary samples are based on SPM and
930 sediments, whereas those of river samples are based only on SPM. Boxes are color-coded based
931 on the sample type (soil in brown, river in red, upstream estuary in yellow, and downstream estuary
932 in blue). Statistical testing was performed by a Wilcoxon test (*P < 0.05; **P < 0.01; ***P < 0.001;
933 ****P < 0.0001; ns, not significant, P >0.05).

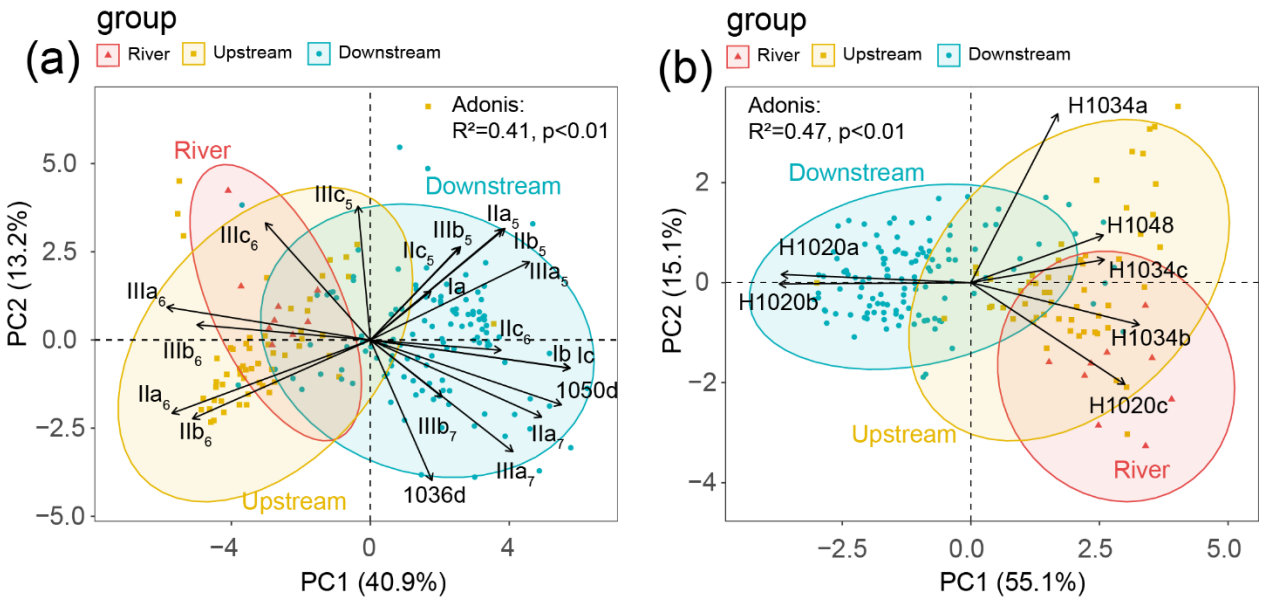

934

935 **Fig. 4.** PCA analysis of fractional abundances of (a) brGDGTs and (b) brGMGTs. The dataset used
936 for PCA analysis is composed of SPM and sediments. Adonis analysis was used to evaluate how
937 variation can be explained by the variables (999 permutations).

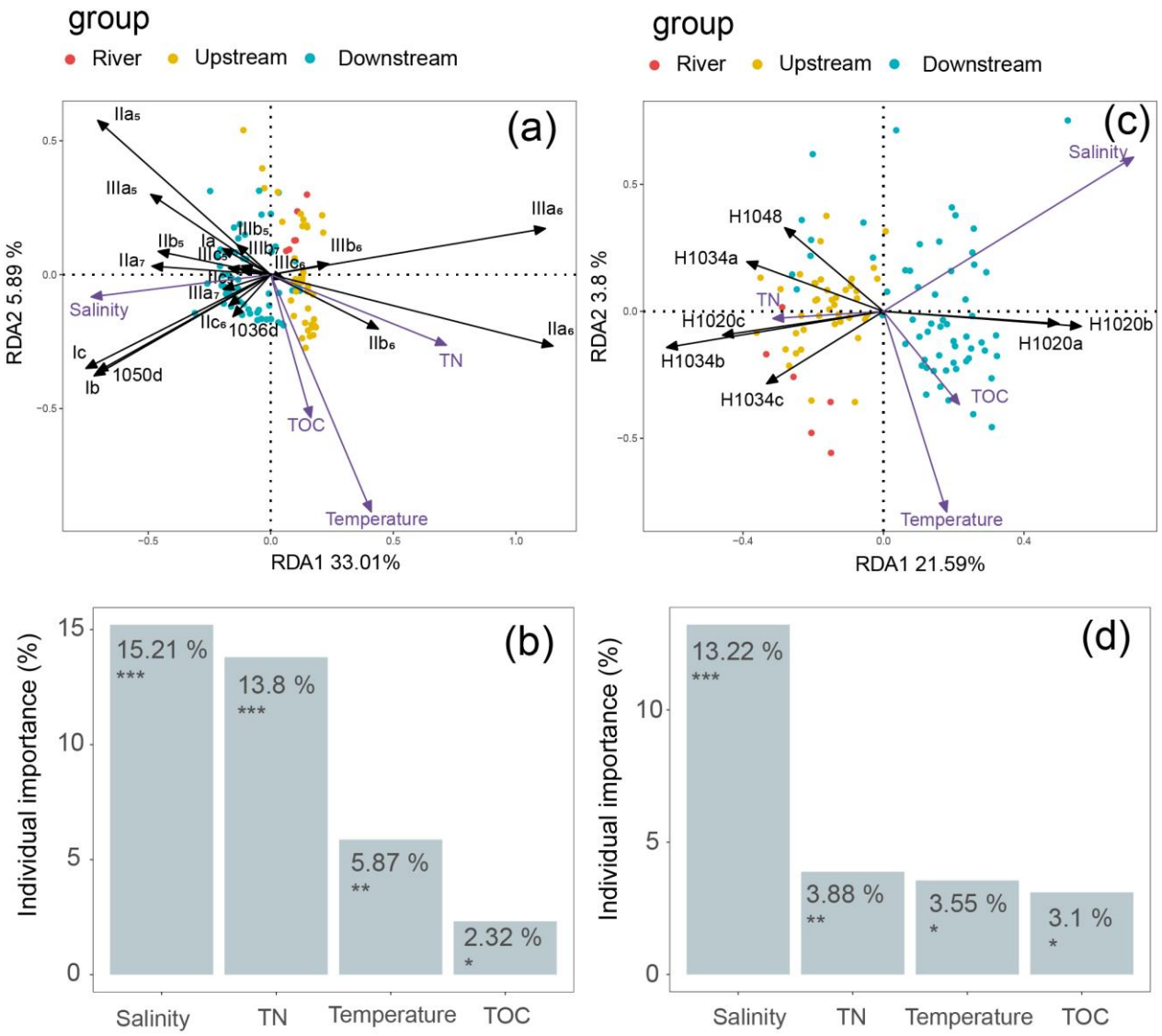

Fig. 5. RDA analysis showing relationships between environmental factors (TN, TOC, salinity, temperature, purple arrows) and fractional abundances of (a) brGDGTs and (c) brGMGTs. The individual importance of the environmental factors (TN, TOC, salinity, temperature) explaining the variation in (b) brGDGT and (d) brGMGT distributions was determined by hierarchical partitioning analysis. The dataset used for RDA analysis is composed of SPM from river (n=6; red), upstream estuary (n=42; yellow), and downstream estuary (n=59; blue). Significance level is indicated by asterisks: *P < 0.05; **P < 0.01; ***P < 0.001.

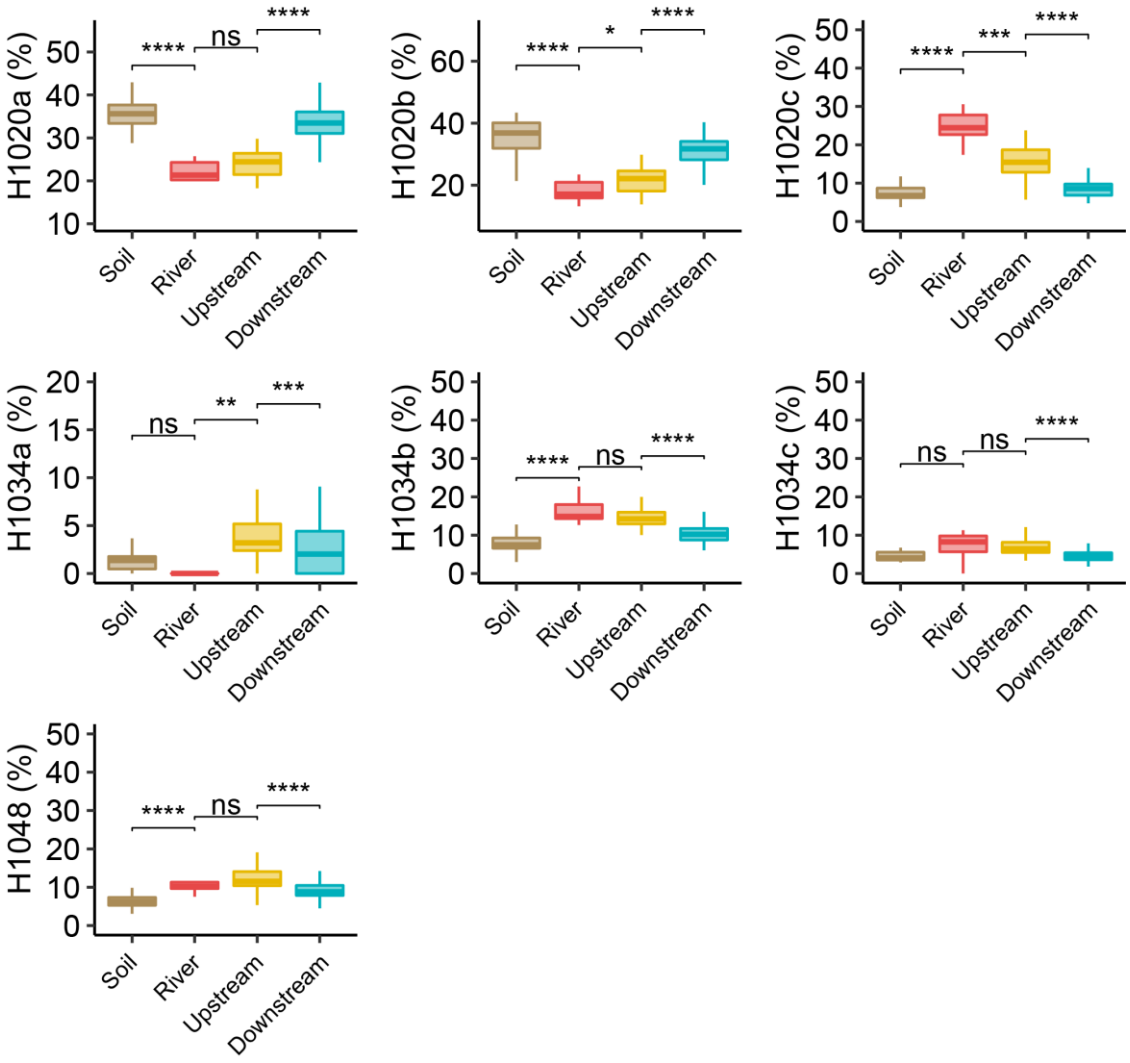

Fig. 6. Relative abundance of distinct brGMGTs from soils (surficial soils and mudflat soils/sediments, *n*=51), river (*n*=9), upstream estuary (*n*=56) and downstream estuary (*n*=121) across the Seine River basin. Box plots of upstream and downstream estuary are composed of SPM and sediments, whereas those of river are composed of SPM. Boxes are color-coded based on the sample type (soil in brown, river in red, upstream estuary in yellow, and downstream estuary in blue). Statistical testing was performed by a Wilcoxon test (*P < 0.05; **P < 0.01; ***P < 0.001; ****P < 0.0001; ns, not significant, P >0.05).

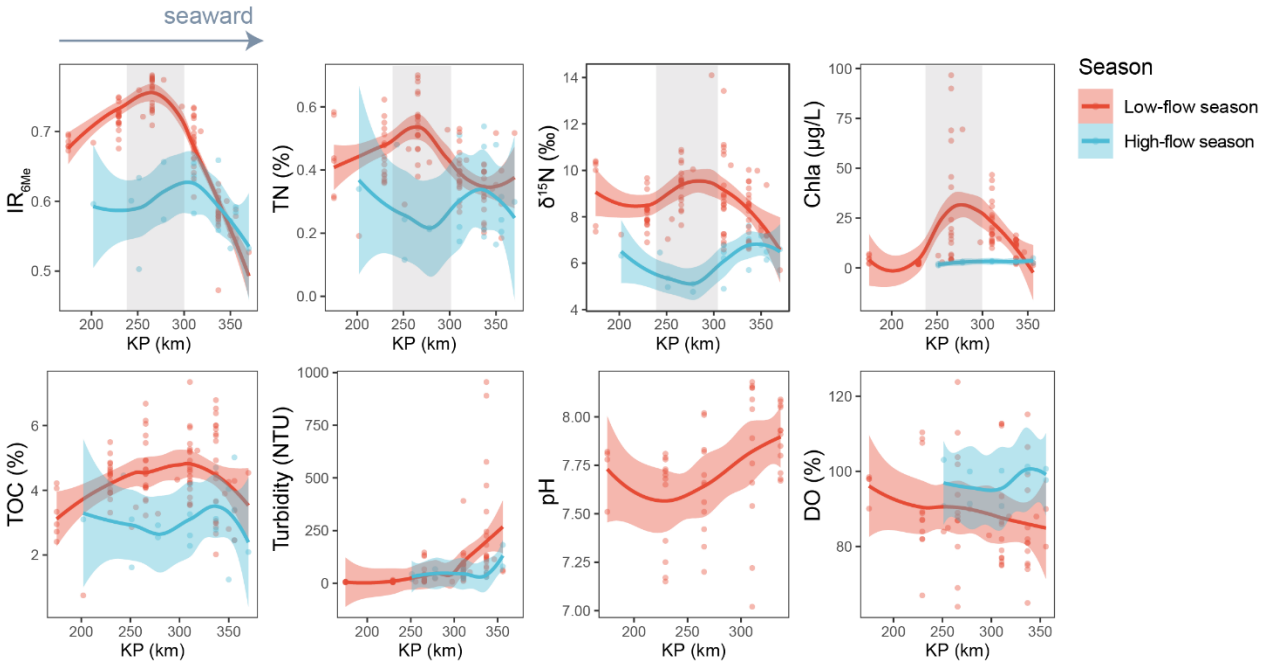

Fig. 7. Spatio-temporal variations of IR_{6Me} and several environmental factors, including TN (%), $\delta^{15}N$ (‰), Chla (µg/L), TOC (%), turbidity (NTU), pH, and dissolved oxygen saturation (DO, %). The trends showing variations were based on locally estimated scatterplot smoothing (LOESS) method with 95% confidence intervals. KP (kilometric point) represents the distance in kilometers from the city of Paris (KP 0). Dataset is composed of SPM. The shaded area highlights a zone (KP 243-297.6) where IR_{6Me} and several environmental parameters co-vary.

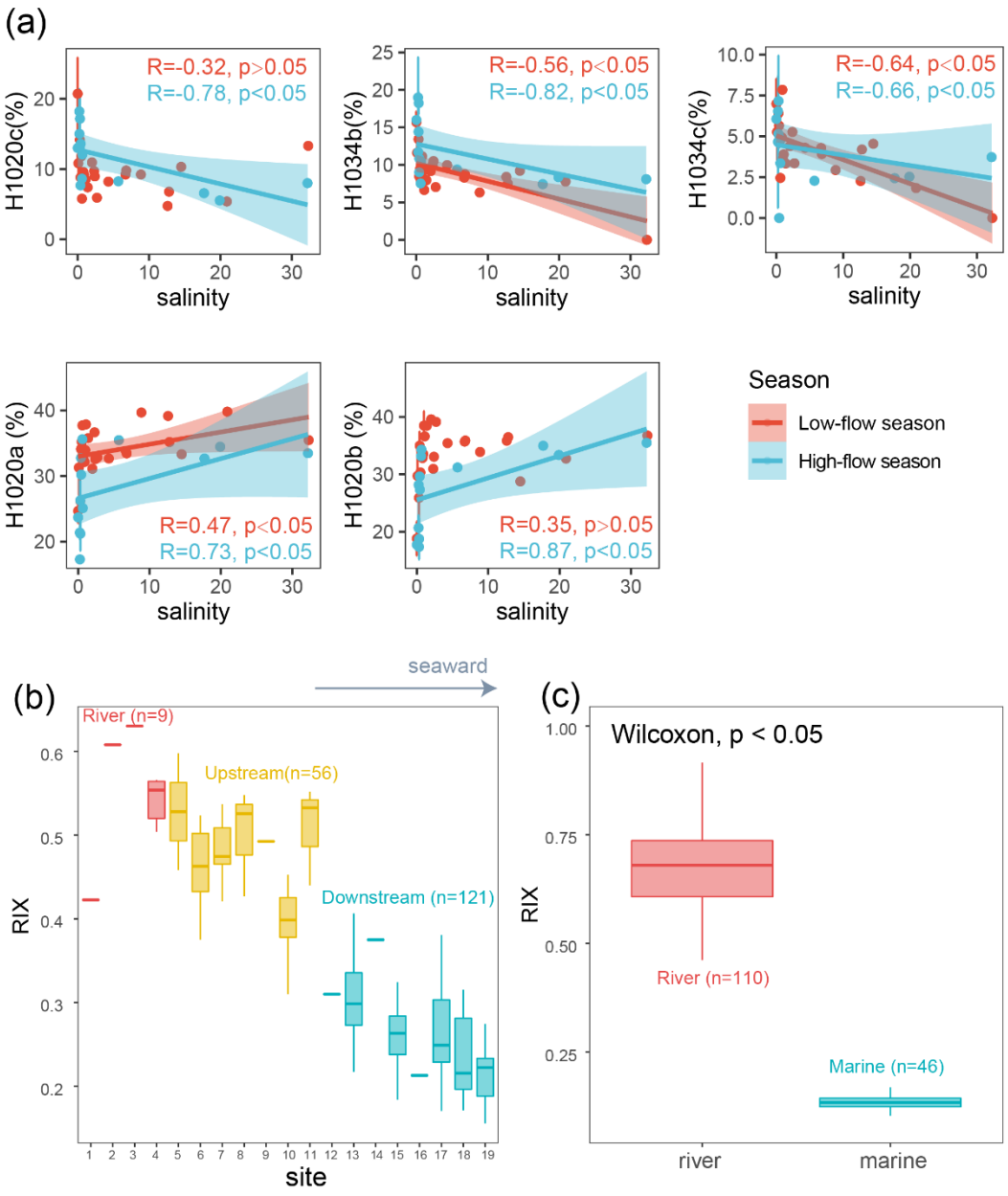

966

967 **Fig. 8.** (a) Salinity plotted versus relative abundance of brGMGTs. Shaded area represent 95%
968 confidence intervals. Vertical error bars indicate mean ± s.d for samples with the same salinity.
969 Dataset is composed of SPM. (b) Distribution of RIX across the Seine River basin. Boxes are color-
970 coded based on the sample type (river in red, upstream estuary in yellow, and downstream estuary
971 in blue). Dataset is composed of SPM and sediments. (c) RIX in the Godavari River basin (India)
972 and Bay of Bengal sediments (data from Kirkels et al. (2022a)). Statistical testing was performed
973 by a Wilcoxon test.

974

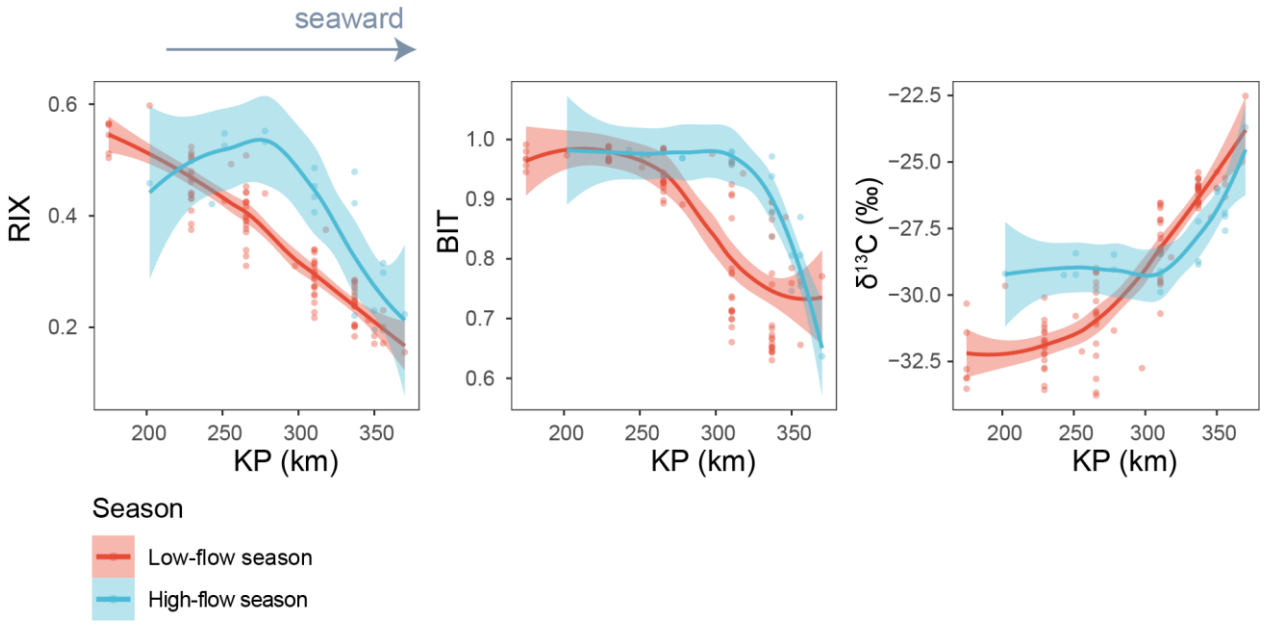

975

976 **Fig. 9.** Spatio-temporal variations of RIX and several other terrestrial proxies, including BIT and
977 $\delta^{13}C$ (‰). The trends showing spatio-temporal variations were based on locally estimated
978 scatterplot smoothing (LOESS) method with 95% confidence intervals. KP (kilometric point)
979 represents the distance in kilometers from the city of Paris (KP 0). Dataset is composed of SPM.

980

981

982

983

984